JHEP PROCEEDINGS

*International Europhysics Conference on HEP*

# Conference Summary

**Günter Wolf***

*Deutsches Elektronen Synchrotron DESY, Hamburg Germany*

*E-mail:* Guenter.Wolf@desy.de

ABSTRACT: Highlights presented at this conference are reviewed. This includes observation of CP violation in the $B$-sector, detection of direct CP violation in the $K^0$-system, new measurements on solar neutrinos, cosmic microwave background radiation and properties of the universe, electroweak results from the large colliders and tests of the Standard Model, measurement of the anomalous magnetic moment of muons, structure of the proton at large energy transfers and virtualities, and heavy ion collisions at very high energies. Finally, the physics reach of TEVATRONII, LHC and TESLA, a linear $e^+e^-$ collider proposed for the 0.5 - 1 TeV regime, is briefly reviewed.



## 1. Introduction

This year has been a splendid year for particle physics. Several outstanding issues have been answered by experiment. The searches for cracks in the Standard Model (SM) have now become so precise that electroweak interactions can be tested at the loop level. This report gives a brief tour of some of the key results presented at this conference.

## 2. CP violation in the B - sector

At this conference, BABAR presented definitive evidence for CP violation in the $B$ system [1, 2]. The environment in which CP violation takes place in $B^0$ mesons is very similar to that for neutral kaons: W exchange mixes $B^0$ and $\overline{B^0}$, see Fig. 1. As a result of mixing, the CP eigenstates are

$$B^0_{1,2} = \frac{1}{\sqrt{2}}(B^0_d \pm \overline{B^0_d}). \tag{2.1}$$

A suitable place to search for CP violation in the $B$ system is the $\Upsilon(4S)$, a CP eigenstate (CP+) which decays close to 50% into $B^0\overline{B^0}$. In the BABAR experiment, the $\Upsilon(4S)$ is produced by $e^+e^-$ annihilation,

$$e^+e^- \to \Upsilon(4S) \to B^0\overline{B}^0. \tag{2.2}$$

*Speaker.

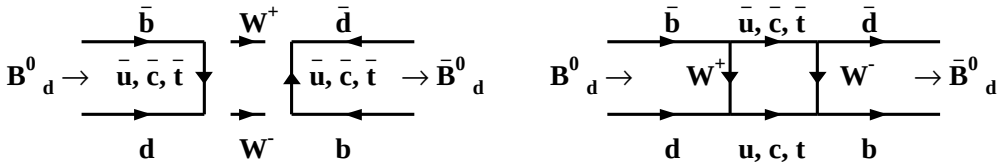


**Figure 1:** Diagrams contributing to $B\overline{B}$ mixing.

The measurement is performed by establishing that one $B$ is either a $B^0$ or a $\overline{B}^0$ (*flavour tag*) and then determining the difference in decay times $\Delta t$ between the flavour tagged $B$ and the other $B$, detected in a final state with definite CP, $B_{CP}$. Examples of final states with definite CP suitable for measuring $\Delta t$ are: $J/\psi K_S^0$ (CP-) and $J/\psi K_L^0$ (CP+). A difference in the $\Delta t$ distribution for $B^0$ and $\overline{B^0}$ is evidence for CP violation:

$$A_{CP}(\Delta t) = \frac{N_{B^0_{tag}}(\Delta t) - N_{\overline{B^0_{tag}}}(\Delta t)}{N_{B^0_{tag}}(\Delta t) + N_{\overline{B^0_{tag}}}(\Delta t)} = -\eta_f \cdot \sin(2\beta) \cdot \sin(\Delta m \Delta t) \tag{2.3}$$

where $\eta_f$ is the CP eigenvalue of the final state $f$, $\Delta m$ is the mass difference between $B_1^0$ and $B_2^0$ and $\beta = arg[-\frac{V_{cd}V_{cb}^*}{V_{td}V_{tb}^*}]$ is one of the angles of the unitary triangle given by the CKM matrix. Candidate events for states with definite CP parity are selected by requiring that the difference between their energy and the beam energy, $\Delta E$, is small, see Fig. 2 (left). For modes involving $K_S^0$, the mass parameter $m_{ES} = \sqrt{(E_{beam}^{cm})^2 - (p_B^{cm})^2}$ is required to be greater than 5.2 GeV.

Figure 2 (right) shows, for the 803 events selected by BABAR, the number of detected $B^0$ ($\overline{B^0}$) with a $\overline{B^0}$ ($B^0$) tag as a function of $\Delta t$. A clear asymmetry is observed in the $\Delta t$ distribution for $B^0$'s with a $\overline{B^0}$ tag, and an opposite asymmetry for $\overline{B^0}$'s with a $B^0$ tag. The value for $\sin(2\beta)$ is

$$\sin(2\beta) = 0.59 \pm 0.14(\text{stat}) \pm 0.05(\text{sys}), \tag{2.4}$$

which establishes CP violation in the $B$ system with 4.1 s.d.

An average over all $\sin(2\beta)$ values measured so far gave [3][1]:

$$\sin(2\beta)_{Data} = 0.62 \pm 0.13 \tag{2.5}$$

which is in good agreement with the SM predictions obtained from a fit of the data for the corresponding CKM unitarity triangle [3, 4]:

$$\sin(2\beta)_{SM} = 0.70 \pm 0.12. \tag{2.6}$$

[1]Inclusion of the result from BELLE, shown later at the Lepton-Photon Conference 2001: $\sin(2\beta)_{BELLE} = 0.99 \pm 0.14(stat) \pm 0.06(sys)$ leads to the average [3]: $\sin(2\beta)_{Data} = 0.79 \pm 0.12$.

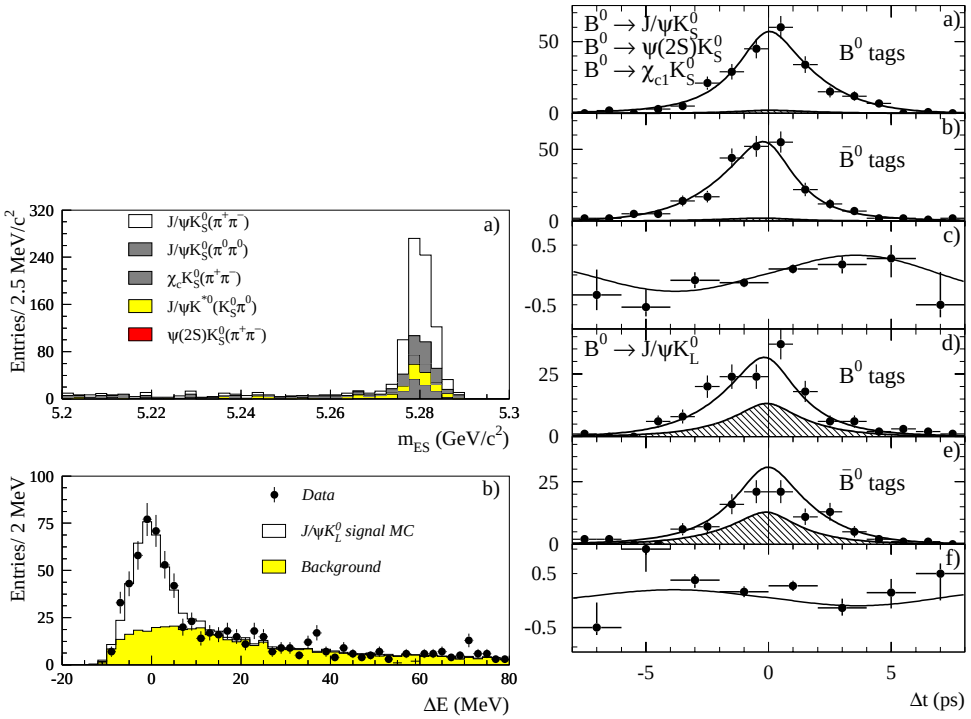


**Figure 2:** Left: Candidate events with definite CP with a final state $K^0_S$ (a) or $K^0_L$ (b). Right: $\Delta t$ distribution for CP- candidates (a) with a $B^0$ tag, (b) with a $\overline{B}^0$ tag and (c) for the asymmetry $(N_{B^0} - N_{\overline{B}^0})/(N_{B^0} + N_{\overline{B}^0})$. The solid curves represent the result of the combined fit. The shaded regions represent background contributions. Figures (d)-(f) contain the corresponding information for CP+ candidates. Figure from BABAR.

## 3. New results from BELLE

The KEK - B factory performs well. A maximum luminosity of 220 pb$^{-1}$ per day has been achieved. The maximum instantaneous luminosity attained has been $4.4 \cdot 10^{33}$cm$^{-2}$s$^{-1}$ which is a factor of 1.5 above design. Figure 3 shows the observations of two strongly suppressed decays: the first one, $B^0 \to D^0\pi^0$ is colour suppressed and has a branching ratio of $(2.6 \pm 0.4) \cdot 10^{-4}$; the second one is a charmless 3-body decay, $B^- \to K^+K^+K^-$, with a branching ratio of $(3.7 \pm 0.4 \pm 0.4) \cdot 10^{-5}$ [5].

The BELLE collaboration has presented first results on CP-violation in the B-sector in Ref. [6] from a sample of 194 $B$ candidates. Results from a data sample which is comparable to that of BABAR will be presented next week at the Lepton - Photon conference.

## 4. CP violation in the $K^0$ system and the value of $\epsilon'/\epsilon$

CP violation in particle decay was observed for the first time in 1964 by [7] in a study of the neutral $K$ system. CP violation was found to occur at the level of $\epsilon = 2.3 \cdot 10^{-3}$. The same type of diagrams which mix $B^0$ and $\overline{B^0}$ are also active in the $K$ system. The question

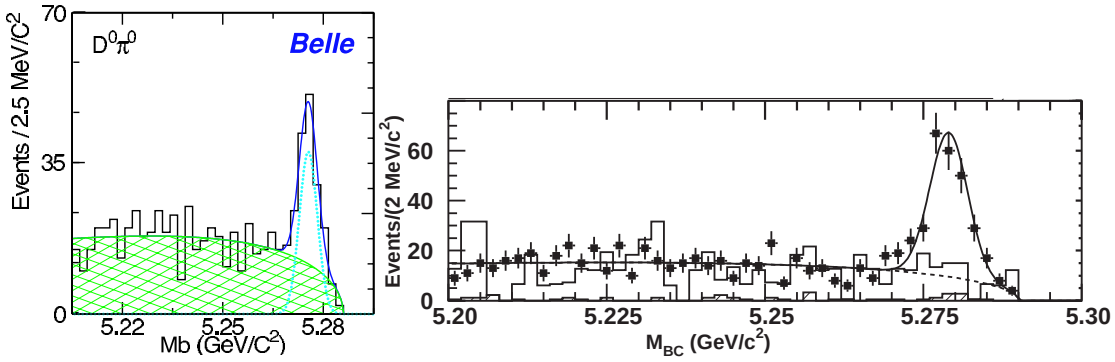


**Figure 3:** Observation of the colour-suppressed decay $B \to D^0\pi^0$ (left) and of the charmless $B^+ \to K^+K^+K^-$ decay (right). From Belle.

then arose whether CP violation is solely due to mixing or whether there is also direct CP violation which may occur, e.g., due to penguin diagrams of the type shown in Fig. 4.

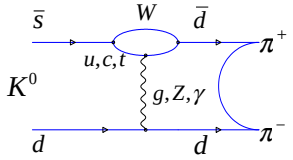


**Figure 4:** A peguin diagram for direct CP-violation in the $K$ system.

The strength of direct CP violation is measured by the complex parameter $\epsilon'$. The determination of $\epsilon'$ required a heroic effort on the experimental side. Direct CP violation manifests itself e.g. in different rates for the two CP violating decays $K_L^0 \to \pi^+\pi^-$ and $K_L^0 \to \pi^0\pi^0$:

$$Re(\epsilon'/\epsilon) = \frac{1}{6}[1 - \frac{\Gamma(K_L \to \pi^0\pi^0) \cdot \Gamma(K_S \to \pi^+\pi^-)}{\Gamma(K_S \to \pi^0\pi^0) \cdot \Gamma(K_L \to \pi^+\pi^-)}]. \tag{4.1}$$

If $\mathrm{Re}(\epsilon'/\epsilon)$ is of the order of $10^{-3}$, then one must detect at least $10^6$ decays for each decay mode. Also, a precise detection of the all-neutral final state $\pi^0\pi^0$ is not the easiest experimental task.

Given these experimental challenges, it is no surprise that the measurement of $\epsilon'$ has been rocky as illustrated by Table 1. The results from the first round of experiments performed at the end of the eighties/beginning of the nineties was inconclusive: E731 found no evidence for direct CP violation, while NA31 observed a positive signal at the level of 3 s.d. This outcome stimulated both groups to a second round of experiments with much larger and more powerful detectors. With a total of 30M and 40M $K^0$ decays, respectively, each of the two experiments, KTeV [8] and NA48 [9], have now established independently the presence of direct CP violation. The average of the two measurements yields

$$Re(\epsilon'/\epsilon) = 1.72 \pm 0.28 \cdot 10^{-3}\ . \tag{4.2}$$

| | | $Re(\epsilon'/\epsilon)$ |
|---|---|---|
| 1993 | E731 | $0.74 \pm 0.59 \cdot 10^{-3}$ |
| 1993 | Na31 | $2.30 \pm 0.65 \cdot 10^{-3}$ |
| 1999 | KTeV (96-97a) | $2.80 \pm 0.41 \cdot 10^{-3}$ |
| 2001 | KTeV reanalysis | $2.32 \pm 0.32 \pm 0.07 \cdot 10^{-3}$ |
| 1999 | NA48 (97) | $1.85 \pm 0.73 \cdot 10^{-3}$ |
| 2001 | NA48 (97-99) | $1.53 \pm 0.26 \cdot 10^{-3}$ |
| | $\pi^0\pi^0$: $K_L$ 3M $K_S$ 5M | |
| | $\pi^+\pi^-$: $K_L$ 14M $K_S$ 22M | |
| 2001 | KTeV (97) | $1.98 \pm 0.17 \pm 0.23 \pm 0.06 \cdot 10^{-3}$ |
| | KTeV (96-97) | $2.07 \pm 0.28 \cdot 10^{-}3$ |
| | $\pi^0\pi^0$: $K_L$ 3M $K_S$ 4M | |
| | $\pi^+\pi^-$: $K_L$ 9M $K_S$ 15M | |

**Table 1:** List of experiments, number of events and results on $Re(\epsilon'/\epsilon)$.

A nonzero value of $Re(\epsilon'/\epsilon)$ excludes the superweak model of Wolfenstein [10]. In the SM the dominant contribution comes from two penguin diagrams (one of which is shown in Fig. 4) which are large and nearly cancel each other. In [11] a range of $(0.2 - 3) \cdot 10^{-3}$ has been predicted for $Re(\epsilon'/\epsilon)$ from SM sources. For a discussion see [12].

## 5. Neutrino mixing

### 5.1 Solar neutrinos

A large number of experiments measuring the flux of neutrinos from the sun have observed less neutrinos than predicted by the Standard Solar Model (SSM). The Sudbury Neutrino Observatory (SNO) has recently joined this field as a new player [13]. The experiment is performed in a mine near Sudbury (Canada) at a depth of 6000 m water equivalent. The active detector consists of 1000 t of heavy water in a cylinder of 6.0 m radius surrounded by normal water up to a radius of about 11 m. Cerenkov radiation generated in the heavy water is read out by 9500 photomultipliers (PMT). On average, about 9 PMTs respond per MeV of electron energy. Signals above an energy $T_{eff} > 6.75$ MeV are used in the final analysis. With a minimum energy cut of 6.75 MeV SNO is only sensitive to $^8B$ neutrinos.

Neutrinos from the sun are observed via three reactions,

$$\nu_e d \to ppe^- \quad \text{CC} \quad 975 \pm 40 \text{ events} \tag{5.1}$$

$$\nu_x d \to \nu_x pn \quad \text{NC} \quad 88 \pm 25 \text{ events} \tag{5.2}$$

$$\nu_x e^- \to \nu_x e^- \quad \text{ES} \quad 106 \pm 15 \text{ events} \tag{5.3}$$

The CC process is only sensitive to $\nu_e$; NC is sensitive to all active flavours and the elastic scattering (ES) is also sensitive to all flavours, but with reduced sensitivity for $\nu_\mu$ and $\nu_\tau$ due to the extra contribution for $\nu_e e^-$ scattering from $W$ exchange.

The final data set contains 1169 events. Figure 5 (a) shows the distribution of the angle $\Theta_{sun}$ between the reconstructed direction of the event and the sun. The observed forward peak is due to elastic scattering (ES). The events outside of the forward peak stem mostly from the CC reaction. Based on the measured $T_{eff}, cos\Theta_{sun}$ and the radial distance of the event vertex, a fit resolves the data into the three categories leading to $975 \pm 40$ CC, $106 \pm 15$ ES and $88 \pm 25$ NC events.

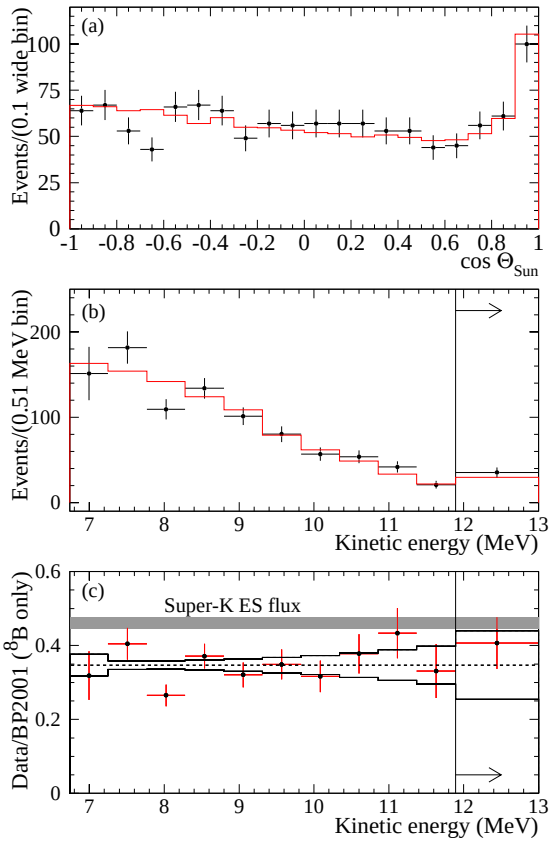


**Figure 5:** SNO results on solar neutrinos: (a) distribution of $\cos\theta$; (b) kinetic energy spectrum for CC events; (c) ratio of the data to the predictions[15] for the kinetic energy distribution.

The electron energy spectrum presented in Fig. 5(b) for CC events peaks at low energies. The histogram shows the spectrum expected from $^8B$ neutrinos scaled to the data. It is in good agreement with the measurement. The resulting $^8B$ neutrino fluxes above 6.75 MeV are

$$\Phi^{CC}_{SNO}(\nu_e) = (1.75 \pm 0.07^{+0.12}_{-0.11} \pm 0.07) \cdot 10^6 \text{ cm}^{-2}\text{s}^{-1} \quad (5.4)$$

$$\Phi^{ES}_{SNO}(\nu_x) = (2.39 \pm 0.34^{+0.16}_{-0.14}) \cdot 10^6 \text{ cm}^{-2}\text{s}^{-1}. \quad (5.5)$$

The ratio of the CC data to the SSM prediction [15] is constant as a function of the kinetic energy, see Fig. 5(c). The average value of the ratio is $0.347 \pm 0.029$: only 34.7% of the $\nu_e$ emitted by the sun are actually observed as $\nu_e$ on earth.

The ES flux from SNO agrees with the more precise result from SUPER-KAMIOKANDE (SK) [14]:

$$\Phi_{SK}^{ES}(\nu_x) = (2.32 \pm 0.03^{+0.08}_{-0.07}) \cdot 10^6 \text{ cm}^{-2}\text{s}^{-1}. \tag{5.6}$$

Using the SK flux for ES, there is a 3.3 s.d excess of the ES over the CC flux,

$$\Phi_{SK}^{ES} - \Phi_{SNO}^{CC} = (0.57 \pm 0.17) \cdot 10^6 \text{ cm}^{-2}\text{s}^{-1}. \tag{5.7}$$

This gives evidence for extra $\nu$'s $\neq \nu_e$ from $^8B$. Since these extra $\nu$'s do, interact they are not sterile! With the addition of these extra neutrinos, the total flux of active $^8B$ neutrinos measured is

$$\Phi(\nu_x)_{meas} = (5.44 \pm 0.99) \cdot 10^6 \text{ cm}^{-2}\text{s}^{-1} \tag{5.8}$$

which is in excellent agreement with the SSM prediction for the total $\nu_e$ flux from $^8B$ [16],

$$\Phi(\nu_x)_{SSM} = (5.05^{+1.01}_{-0.81}) \cdot 10^6 \text{ cm}^{-2}\text{s}^{-1}. \tag{5.9}$$

The combined SK + SNO data show that the total sun $\nu$ flux expected from $^8B$ is indeed observed on earth: about one third as $\nu_e$ and two thirds as active $\nu$'s with different $\nu$ flavour(s). This is the first direct indication of a non-electron flavour component in the solar neutrino flux.

The agreement of the flux predicted by the SSM with the measurements is also an impressive success for the SSM calculation of the $^8B$ flux which depends on the 18th power of the temperature of the sun, $\Phi_{SSM}^{8B} \propto T_{sun}^{18}$ [17].

Figure 6 shows, from a recent analysis of SK for $\nu_e - \nu_\mu(\nu_\tau)$ oscillations, the $\Delta m^2, sin^2(2\theta)$ regions excluded by the zenith angle spectrum of SK, and the allowed regions from a global fit to the data from the CL, GA, HOMESTAKE and SK flux measurements [13, 18]. The small angle and vacuum (or just so) oscillation solutions are now disfavoured at the 95% C.L. The only allowed region left has approximately $0.6 < sin^2(2\theta) < 0.9$ and $\Delta m^2 = 3{\cdot}10^{-5} - 2{\cdot}10^{-4}$ eV$^2$.

### 5.2 Atmospheric neutrinos

The latest results on $\nu_\mu - \nu_\tau$ oscillations from a combined fit to the SK, GALLEX, SAGE and HOMESTAKE data yield $\Delta m^2 = 2.5 \pm 0.4 \cdot 10^{-3}$ eV$^2$ ($\Delta m^2 > 1.2 \cdot 10^3$eV$^2$ at 95 % C.L. and $sin^2 2\theta$ close to unity) [14, 18].

### 5.3 LSND effect

Figure 6 (right) shows, in the ($\Delta m^2$, $sin^2 2\theta$) plane, the regions for $\nu_X - \nu_Y$ oscillations indicated by the LSND experiment at Los Alamos. A new measurement performed at RAL, KARMEN II [19], found no evidence for the LSND effect, viz. 11 events observed,

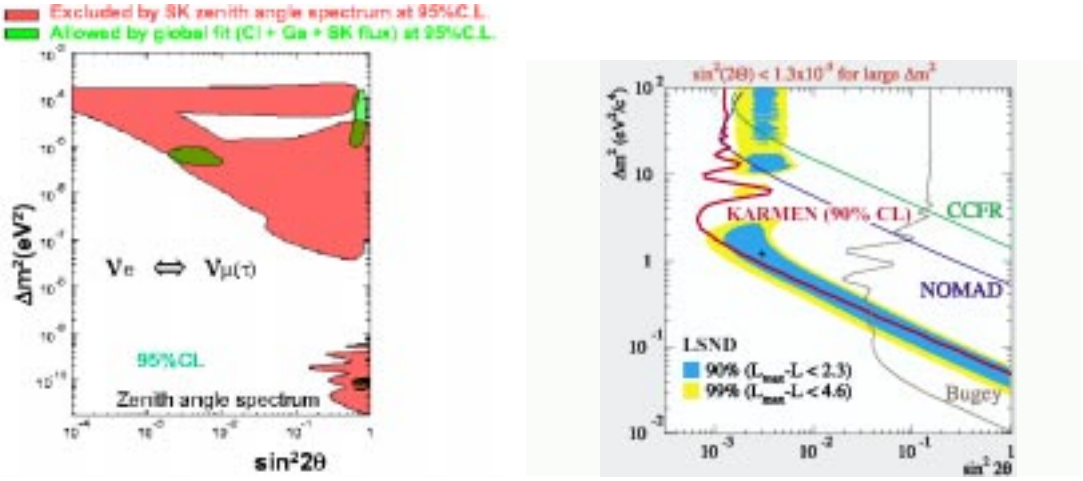


**Figure 6:** Left: Results on $\nu_e - \nu_{\mu(\tau)}$ oscillations in the $\Delta m^2$ versus $\sin^2(2\theta)$ plane. From SK. Right: LSND effect and new KARMEN results. From [19].

compared to $12.3 \pm 0.6$ events expected from standard sources. This excludes most of the LSND signal region. A definitive answer can be expected from the MINIBOONE experiment planned at Fermilab which should observe 1000 events/year if the LSND signal is real.

### 5.4 $\nu_e$ mass

The Mainz experiment [20] presented a direct measurement of the $\nu_e$ mass from the tritium beta decay experiment yielding $m_{\nu_e} < 2.2$ eV (95% C.L.) which can be compared with the Troitsk result of $m_{\nu_e} < 2.5$ eV (95% C.L.) [21]. A next generation detector (KATRIN: length about 60 m) is on the drawing board promising sensitivity down to $m_{\nu_e} = 0.3$ eV [22].

## 6. Neutrino factories

Assuming three neutrino flavours, a CKM-type matrix, with three angles, $\theta_1, \theta_2, \theta_3$ and one phase $\delta$ will provide the most general description, see e.g. [23, 24] at this conference:

$$\begin{pmatrix} \nu_e \\ \nu_\mu \\ \nu_\tau \end{pmatrix} = \begin{pmatrix} c_1c_3 & s_1c_3 & s_3 \\ -c_1s_2s_3 - s_1s_2s_3 & -c_1c_2e^{-i\delta} - s_1c_2e^{-i\delta} & s_2c_3 \\ -c_1c_2s_3 - s_1s_2e^{-i\delta} & -s_1c_2s_3 - c_1s_2e^{-i\delta} & c_2c_3 \end{pmatrix} \begin{pmatrix} 1 & 0 & 0 \\ 0 & e^{i\rho} & 0 \\ 0 & 0 & e^{i\sigma} \end{pmatrix} \begin{pmatrix} \nu_1 \\ \nu_2 \\ \nu_3 \end{pmatrix}$$

Here $c_i$, $s_i$ stand for $cos\theta_i$, $sin\theta_i$. The angles $\theta_i$ might be affected by the MSW effect [25] which the $\nu_e$ experiences on its passage through matter. The $\rho$ and $\sigma$ are Majorana phases which can be rotated away [26].

Judging from the experience with the CKM matrix for quarks, it will take massive efforts to reach in the $\nu$ sector the type of sensitivity necessary for observing new physics. New accelerator long base line experiments are under construction (FERMILAB-MINOS,

CERN/Gran Sasso-OPERA) which will be sensitive to $\nu_\mu$ disappearance and $\nu_\tau$ appearance, respectively.

In the U.S.[27], in Japan[28] and in Europe[29], studies for high intensity neutrino factories are underway. Plans for the Japan Hadron Facility (JHF) include a high-intensity conventional neutrino beam. The basic idea is to produce an intense multi-GeV beam of muons decaying into $e, \nu_e, \nu_\mu$. Due to the small value of the muon mass, the intrinsic angular spread of the $\nu$'s is small ($p_{T_\mu} \leq m_\mu/3$ and hence $\Delta\theta_\mu \leq \frac{m_\mu/3}{p_\mu}$) which is essential for achieving a high interaction rate in the far detector of a long base line experiment.

The $\nu$ factory studied at CERN is shown in Fig. 7. Protons are accelerated to 2.2 GeV, accumulated for bunching and sent to a target where pions are produced which subsequently decay into muons. The muons are cooled in order to reduce their transverse momentum spread and are then accelerated to 10 - 50 GeV. In the decay ring, for instance for $\mu^+$ decay into $e^+\nu_e\overline{\nu_\mu}$ oscillations, $\nu_e \to \nu_\mu$, will show up as the appearance of wrong sign $\mu$'s. Matter effects, which become substantial for base line distances larger than $\approx$ 1000 km, will allow determination of the sign of $\Delta m^2$ for $\nu_e \to \nu_\mu$ and $\nu_e \to \nu_\tau$ oscillations.

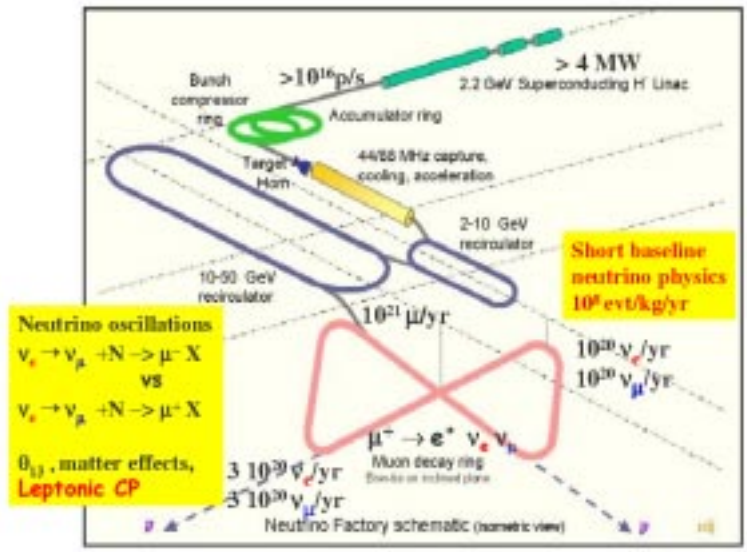


**Figure 7:** Layout of the CERN neutrino factory.

The $\nu$ intensities foreseen are of the order of $10^{20}\nu_e(\nu_\mu)$/year which produce $10^8$ events/kg/year in a near detector! This is an enormous rate - but so are the technical challenges for building such a machine. As an example, the proton beam is a factor of 1000 more intense than achieved with the CERN PS. Also, there is no target yet which will survive such high proton currents. The cooling of the produced muons is another aspect which requires intensive research and development.

## 7. Cosmic Microwave Background

The cosmic microwave background radiation (CMBR) allows us to look back at the early Universe some 14 Gyrs ago. The decisive event occurred about $t_{CMB} = 400000$ years after the big bang when most electrons bound together with protons to form hydrogen. At this point the Universe became transparent to photons. The photons presented a plasma which was inhomogeneous because photon-baryon interactions lead to differences in the photon energy spectra. These photons can be observed today on earth as microwave radiation.

The angle $\theta$ subtended by the microwave emitting Universe cannot be larger than the diameter of the horizon at $t_{CMB}$ seen $t_0 \approx 14$ Gyr later:

$$\theta \propto \frac{1}{1+z}^{1/2} \approx \frac{1}{z}, \tag{7.1}$$

where $z \approx 1200$ is the red shift of light coming to us from these early times.

The existence of CMBR was demonstrated in 1964 by Penzias and Wilson [35]. In 1992, COBE [36] measured the black body temperature of CMB for which the latest measurements give $T_{\rm CMBR}(t_0) = 2.725$ K which is the result of a black body temperature of $T(t_{CMB}) \approx 3000$K.

One can learn more from the CMBR by studying the anisotropies in the temperature, $T$, of the CMBR. By expanding these anisotropies in terms of multipoles,

$$\Delta T(\alpha, \delta) = \sum_{l,m} a_{lm} Y_l^m(\alpha, \delta), \tag{7.2}$$

the averages $c_l =< a_{lm}^l >$ describe the power spectrum of the anisotropies [32]. Peaks in the angular power spectrum of the CMBR were predicted in 1970 [33, 34].

Figure 8 displays the CMBR power spectrum from a recent compilation of the data from DASI, BOOMERanG and MAXIMA[30]. They show a prominent peak around $l_1 = 220$. The strength of this first peak gives evidence for coherent acoustic oscillations with a wave length of the size of the horizon at the time $t = t_{CMBR}$.

The first peak is expected to occur at $l_1 = \frac{2\pi z^{1/2}}{\Omega^{1/2}}$. $\Omega = 1$ describes a flat universe, $\Omega < 1$ an open and $\Omega > 1$ a closed universe. For a flat universe, the first peak in the power spectrum is expected near $l = 220$, in close agreement with the experimental observation. A recent analysis of the CMBR data gives [31, 30]

$$\Omega = 1.03 \pm 0.06. \tag{7.3}$$

It appears that we are living in a flat universe. The combined data suggest the presence of a second peak around $l_3 \approx 2 \cdot l_1 \approx 500$. The presence of such a second peak is a hint for adiabatic acoustic oscillations.

The density of baryons, $\Omega_b$, in the universe affects the balance between pressure and gravity: a larger value of $\Omega_b$ leads to deeper minima between the peaks. The height of the first peak, compared to the dip between the peaks $l_1$ and $l_3$, indicates that $\Omega_b$ is small. The data yield [30]:

$$\Omega_b = (0.021 \pm 0.003)/h^2 \ , \tag{7.4}$$

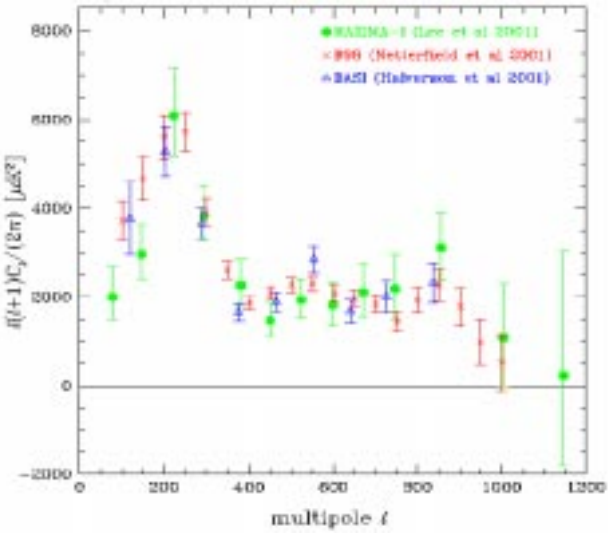


**Figure 8:** CMBR multipole spectra measured by BOOMERanG, Dasi and Maxima.

where $h$ is the Hubble parameter, $h = 0.65 \pm 0.05$. The value found for $\Omega_b$ is consistent with the value obtained from big bang nucleosynthesis.

## 8. Electroweak results from LEP, SLC and the Tevatron

In a splendid performance LEP2 has reached a maximum c.m. energy of $E_{cm} = 208.6$ GeV for $e^+e^-$ - collisions [42, 43]. Figure 9 (left) summarizes the LEP measurements of the total cross section for $e^+e^- \to hadrons$ as a function of $E_{cm}$ together with results from other $e^+e^-$ colliders. The LEP experiments also provided a precise measurement of the cross section for $e^+e^- \to W^+W^-$ from threshold up to 208 GeV (Fig. 9 (right)). This cross section is the result of a delicate interplay between three different contributions: photon and $Z$ exchange in the $s$-channel and $\nu$ exchange in the $t$-channel (Fig. 10). The curves labelled 'no $ZWW$ vertex' and 'only $\nu_e$ exchange' show that without the contribution from the triple gauge vertex $ZWW$ the cross section would diverge.

During 1999 - 2000 the LEP machine team and the four experiments had staged an all out effort in the search for the direct production of the Higgs via $e^+e^- \to ZH$. With a total luminosity of about 546 pb$^{-1}$ in the energy region $E_{cm} = 206 - 208.6$ GeV, the combined data show a tantalizing hint for a Higgs with mass 115.6 GeV [44], see Fig.11 (left). The majority of the events in the signal region stem from one experiment (ALEPH). The probability for the excess to be a statistical fluctuation of the background is 3.4%. Unfortunately, further data taking for either substantiating or dismissing the evidence was not possible. The combined 95% C.L. lower limit from the four LEP experiments is $M_H = 114.1$ GeV. In Fig. 11 (right), this limit is compared with the theoretical prediction.

Figure 12 left lists the recent results for the $W$ mass. The direct measurements from LEP2 and the Tevatron are in close agreement yielding an average of $M_W = 80.451 \pm 0.033$ GeV. The indirect measurements lead to $M_W$ values which are lower by about 80 - 90

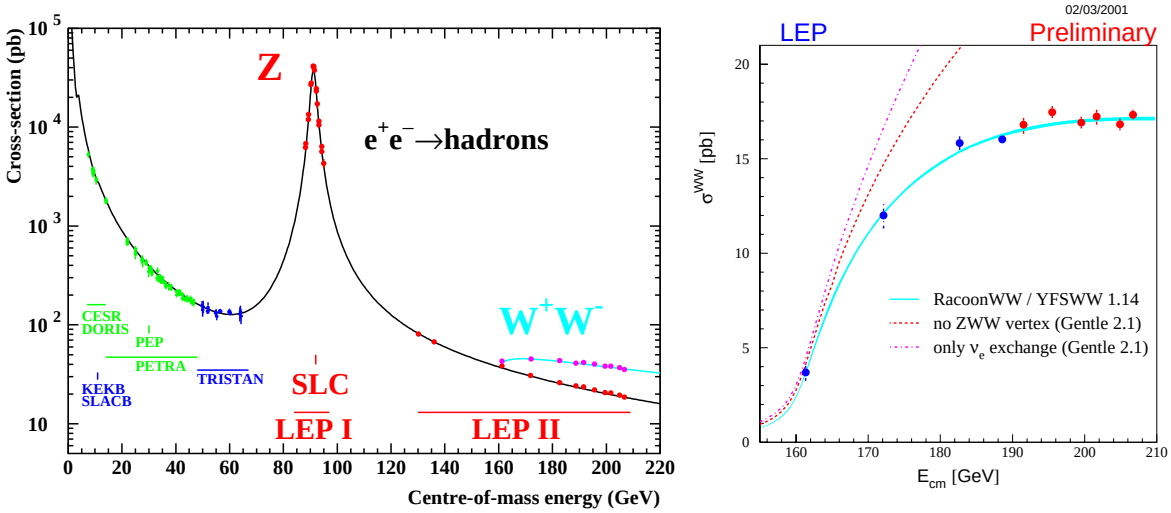


**Figure 9:** Left: The total cross section for $e^+e^-$ annihilation into hadrons. Right: The cross section for $W$-pair production by $e^+e^-$ annihilation.

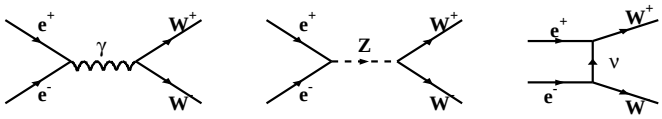


**Figure 10:** Diagrams for $e^+e^- \to W^+W^-$ .

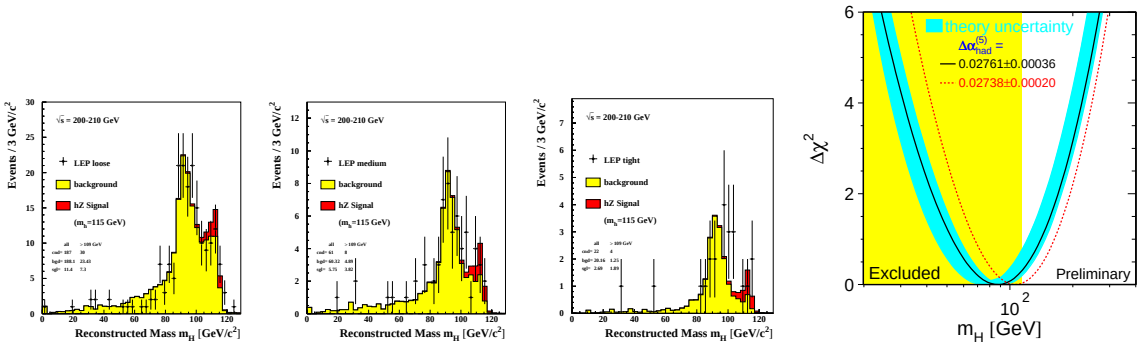


**Figure 11:** Left: Distribution of the reconstructed Higgs mass from three selections with increasing purity of a signal from a 115 GeV Higgs. Right: The theoretical prediction for the Higgs mass in terms of $\Delta\chi^2$ and the mass region excluded by ALEPH, DELPHI, L3 and OPAL (shaded band).

MeV, on average, with a significance of 2 s.d. These indirect measurements are based primarily on the relation $M_W^2 = (1 - sin^2\theta_W)M_Z^2$, where the mass of the $Z$ and $sin^2\theta_W$ are

taken from the data. Figure 12 (right) summarizes the results for $sin^2\theta_{eff}$ (which differs from $sin^2\theta_W$ due to higher order contributions). The lepton final states are seen to give smaller $sin^2\theta_{eff}$ values than those with heavy quarks. The $sin^2\theta_{eff}$ measurements with the smallest errors stem from SLD using the polarisation asymmetry $A_l$ for leptons, and from LEP, using the forward-backward asymmetries $A_{FB}$ for $b$ and $c$ quarks. The $sin^2\theta_{eff}$ value deduced from $A_l$ is by $0.00128 \pm 0.00041$ smaller than the result from the heavy quark asymmetries and leads to a $M_W$ value which agrees with the direct measurement. Although the observed differences for $sin^2\theta_{eff}$ (and hence for $M_W$) between the lepton and the heavy quark asymmetries may well be due to statistical fluctuations, it might be worthwhile to check whether there are experimental or theoretical corrections missing for the heavy quark measurements.

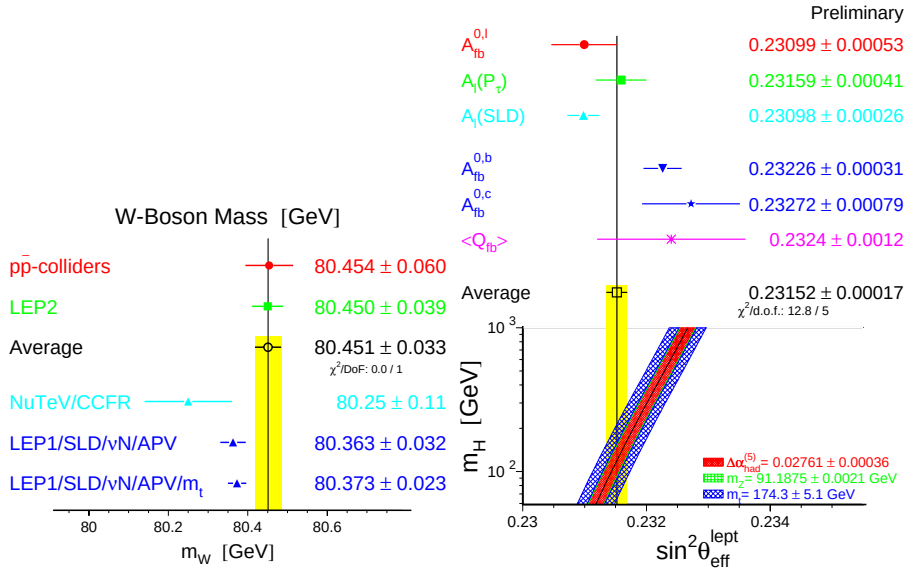


**Figure 12:** Left: Summary of direct (top two) and indirect measurements (bottom three) of the $W$ mass. Right: Summary of $sin^2\theta^{lept}_{eff}$ measurements and the SM prediction for the Higgs mass versus $sin^2\theta^{lept}_{eff}$.

Figure 13 (left) shows a plot of $M_W$ versus the top mass, $M_t$, together with the 68% C.L. contours obtained from the direct and indirect measurements of $M_W$. The two contours are barely touching each other. Also shown are lines for a fixed Higgs mass, $M_H$. The direct measurements favour small $M_H$ values: $M_H < 114$ GeV with about 68% C.L. It is interesting to note that SUSY contributions can possibly raise the value of $M_W$ for fixed $M_t$ [45, 46, 47], e.g., such that in Fig. 13 (left) the 68% C.L. contour from the direct measurement lies now between $M_H = 110$ and 400 GeV, see Fig. 13 (right) taken from [46]. We may see here an experimental hint for physics beyond the SM!

The LEP data limit severely the parameter space for SUSY. This is illustrated in Fig.14 which shows in terms of the neutralino mass versus $\tan\beta$ the regions excluded by LEP, see also [48]. In MSSM, neutralino masses below 45 GeV are excluded for $\tan\beta < 20$. Limits

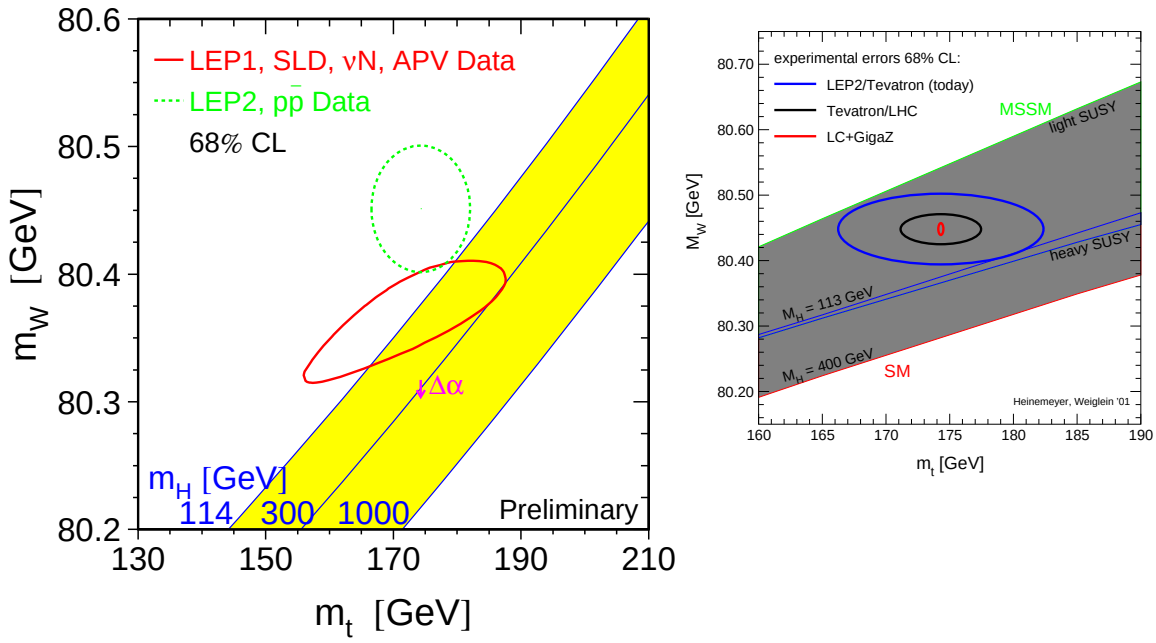


**Figure 13:** $W$-mass versus top-mass. Left: 68% C.L. contours determined by various experiments from direct and indirect measurements of $M_W$, $M_t$, and the SM predictions with Higgs production for different $M_H$. Right: Predictions for $M_W$ versus $M_{top}$ for $M_H$ in the range 114 - 400 GeV from SM (lower band) and MSSM (upper band). For both bands the lower (upper) boundary is for $M_H = 400$ GeV ($M_H = 114$ GeV).

on mSUGRA with $R_p$ - violation from HERA, LEP and the TEVATRON are summarized in Fig. 15.

## 9. Brookhaven $g_\mu - 2$ experiment

A window to new physics is provided by a recent BNL measurement of the muon anomalous magnetic moment at the 1 ppm level [49, 50]. Positive muons are stored in a magnetic ring. When the $\mu^+$ decays, the direction of the emitted $e^+$ is correlated with the direction of the muon spin. The number of $e^+$ is shown in Fig. 16 as a function of time. The experiment is able to follow more than 100 precession cycles of the muon spin.

The measured value for the anomalous magnetic moment, $a_\mu = (g_\mu - 2)/2$, is

$$a_\mu(\text{Data}) = 11\ 659\ 202(14)(6) \cdot 10^{-10} \tag{9.1}$$

This can be compared with the SM value given in [51]:

$$a_\mu(\text{SM}) = 11\ 659\ 159.6(6.7) \cdot 10^{-10}. \tag{9.2}$$

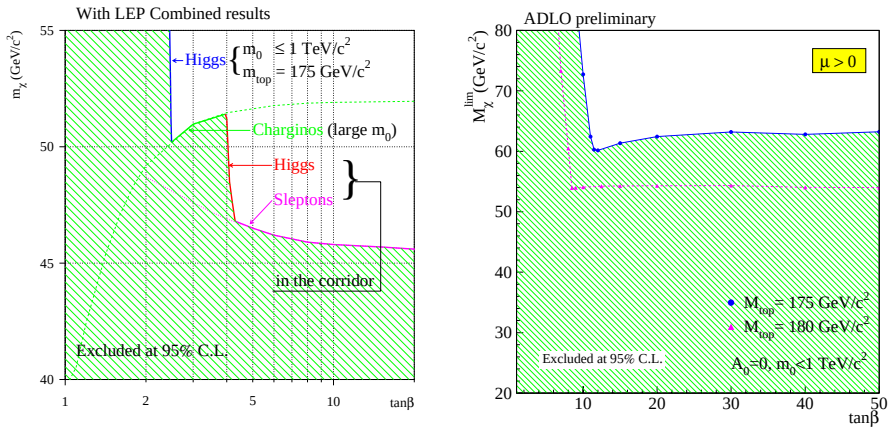


**Figure 14:** Limits from LEP on SUSY. Left: General MSSM LSP neutralino limits assuming only GUT unification without $\tilde{\tau}$ mixing. Right: mSUGRA neutralino LSP mass limit from: the $Z$-width, the search for charginos and sleptons assuming $\tilde{\tau}$-mixing.

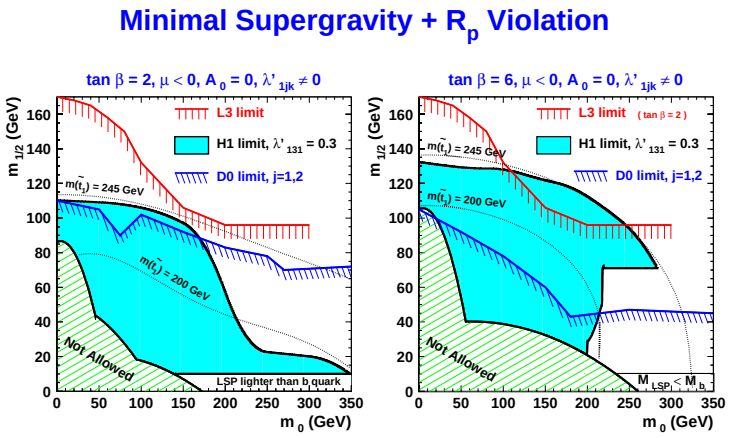




**Figure 15:** Limits from HERA, LEP and TEVATRON on mSUGRA with $R_p$ - violation. The LSP is allowed to decay into a lepton ($e$ or $\nu_e$) and two jets.

The measured value of $a_\mu$ is larger than the SM predictions given in [51] by $(43 \pm 16) \cdot 10^{-10}$. The prediction for $a_\mu$ in the SM depends critically on non-perturbative hadronic contributions. In deriving $a_\mu$(SM), the contribution, from light-by-light scattering has been taken to be:

$$\Delta a_\mu^{Had}(\text{light} - \text{by} - \text{light}) = -8.5(2.5) \cdot 10^{-10}. \tag{9.3}$$

Recent analyses, however, assert $\Delta a_\mu^{Had}(\text{light} - \text{by} - \text{light})$ to be positive [52] and of the value $+8.3(1.2) \cdot 10^{-10}$ [53] which would reduce the discrepancy between data and SM to $(25 \pm 16) \cdot 10^{-10}$ corresponding to a 1.6 s.d. effect only. For a discussion of the SM predictions, see also Ref. [54, 55].

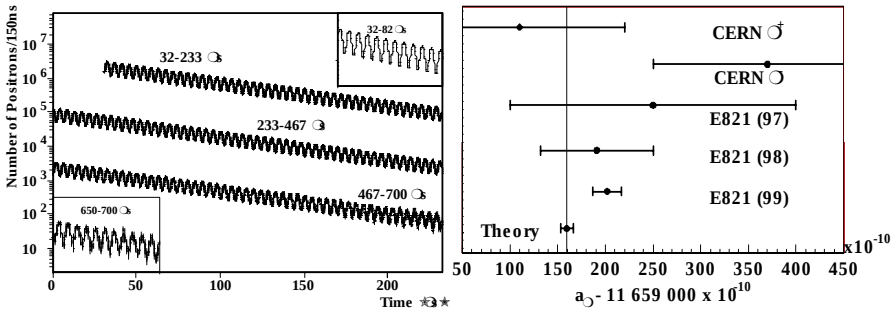


**Figure 16:** Results of the BNL (g-2)-experiment (left) and comparison with other experiments (right).

Contributions from SUSY may lead to deviations from the SM expectations [56]. Taken at face value, the data prefer $\tan\beta = 4 - 40$ which implies chargino masses of 120 - 400 GeV. More data from $\mu^+$, and also from $\mu^-$, are eagerly awaited.

## 10. HERA results

HERA is a giant microscope which allows one to X-ray protons, quarks and leptons and provides a vast testing ground for QCD. Electrons (positrons) of 27.6 GeV collide with 920 GeV protons. The collider experiments H1 and ZEUS have each logged data from integrated luminosities of more than 100 pb$^{-1}$. Inclusive deep inelastic scattering (DIS) can be described by the square of the four-momentum, $-Q^2 = (e - e')^2$ of the exchanged current ($J$) and the energy transfer $\nu$ from the electron to the proton as measured in the proton rest system, Fig. 17 (left). The struck quark carries a momentum fraction $x = \frac{Q^2}{2m_p\nu}$ of the proton (with mass $m_p$). Small-$x$ scattering in the proton rest system is illustrated in Fig.17 (right). For $Q^2 = 15$ GeV$^2$, $x = 2 \cdot 10^{-4}$ corresponds to an energy of the virtual photon $\gamma^*$ of $\nu \approx 40\,000$ GeV. The photon fluctuates into a $q\overline{q}$ system which develops into an almost macroscopic quark-gluon cascade with lifetime $\Delta t = m_p x = \frac{1}{\Delta L} \approx \frac{1}{1000\text{ fm}}$ and transverse size $\Delta d = (Q/\nu)\Delta L = 2/Q \approx 0.1$ fm. The parton with the lowest transverse momentum, $p_t$ of the order of 0.3 GeV, is expected to interact with the proton.

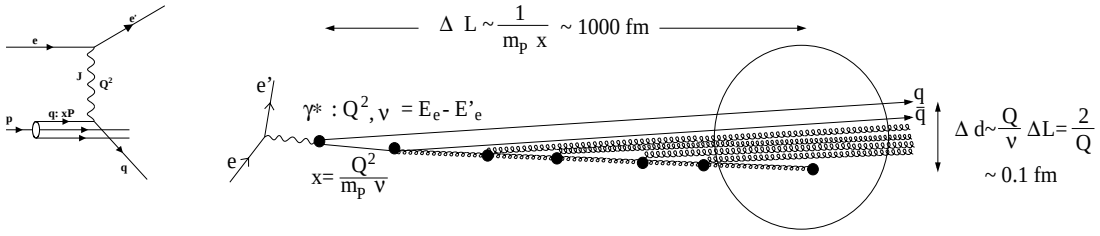


**Figure 17:** Deep inelastic scattering in lowest order (left) and QCD cascade as seen in the proton rest system (right).

For $Q^2 < 1000$ GeV$^2$, the neutral current cross section is dominated by photon exchange leading to

$$\frac{d^2\sigma}{dxdQ^2} = \frac{2\pi\alpha^2}{xQ^4}[1+(1-y)^2]\mathcal{F}_2(x,Q^2)\cdot(1-\delta_L), \tag{10.1}$$

where $\delta_L$ accounts for the contribution from longitudinal photons which, in general, is small. The structure function $\mathcal{F}_2$ can be expressed in terms of the quark densities $q(x,Q^2)$ of the proton in the infinite momentum frame: $\mathcal{F}_2 = \sum_q e_q^2 xq(x,Q^2)$, where $e_q$ is the electric charge of quark $q$. Figure 18 shows $\mathcal{F}_2$ as a function of $\nu$ and $x$ at $Q^2 = 15$ GeV$^2$. For small energy transfers, $50 < \nu < 300$ GeV ($0.15 > x > 0.025$), $\mathcal{F}_2$ is rather constant. Towards larger $\nu$ (smaller $x$), the HERA data show a rapidly rising $\mathcal{F}_2$ which is equivalent to a rapid rise of the parton densities as $x \to 0$.

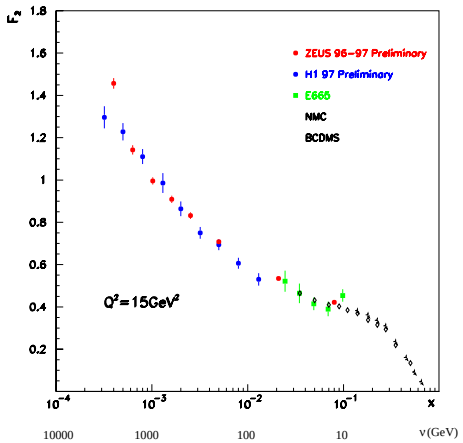


**Figure 18:** The structure function $F_2$ at $Q^2 = 15$ GeV$^2$ as measured by H1 and ZEUS and in fixed target experiments. The bottom scale shows the energy transfer $\nu$ from the electron to the proton measured in the proton rest system.

In Fig. 19, the $\mathcal{F}_2(x,Q^2)$ measurements from HERA are summarized for fixed $Q^2$ values between 0.1 and 150 GeV$^2$ [57, 58]. The transition from a hadronic behaviour, $\mathcal{F}_2 \propto$ const at $Q^2 < 0.6$ GeV$^2$, to a parton-dominated regime at $Q^2 \geq 3$ GeV$^2$ is clearly seen. The rise of $\mathcal{F}_2$ as $x \to 0$ is accelerated with increasing $Q^2$. It is equivalent to a strong rise of the total $\gamma^* p$ cross section as a function of the hadron c.m. energy $W \approx \sqrt{Q^2/x}$: $\sigma^{tot}_{\gamma^* p} \propto W^{2\lambda}$ with $\lambda > 0.2$ for $x < 0.01$, $Q^2 > 10$ GeV$^2$ which is much stronger than for total hadron hadron cross sections. At high $Q^2$, the rise is well described by QCD evolution [59] which requires as input the parton densities as a function of $x$ for *one* fixed value of $Q^2 = Q_0^2$ and then predicts $\mathcal{F}_2(x,Q^2)$ for other values of $Q^2$. At small $Q^2$ the rise is reduced presumable due to confinement forces.

From the change of $\mathcal{F}_2$ with $Q^2$ one determines the gluon density $g(x,Q^2)$ of the proton: $xg \propto \frac{d\mathcal{F}_2}{d\ln Q^2}$ for small $x$ [60]. A precise determination is obtained from a QCD-DGLAP fit to the $\mathcal{F}_2$ data [57, 61]. Figure 20 (left) shows the resulting $xg(x,Q^2)$ for $Q^2 = 5, 20$ and 200 GeV$^2$. An $x$ behaviour very similar to that of $\mathcal{F}_2$ - i.e. similar to that of the quark

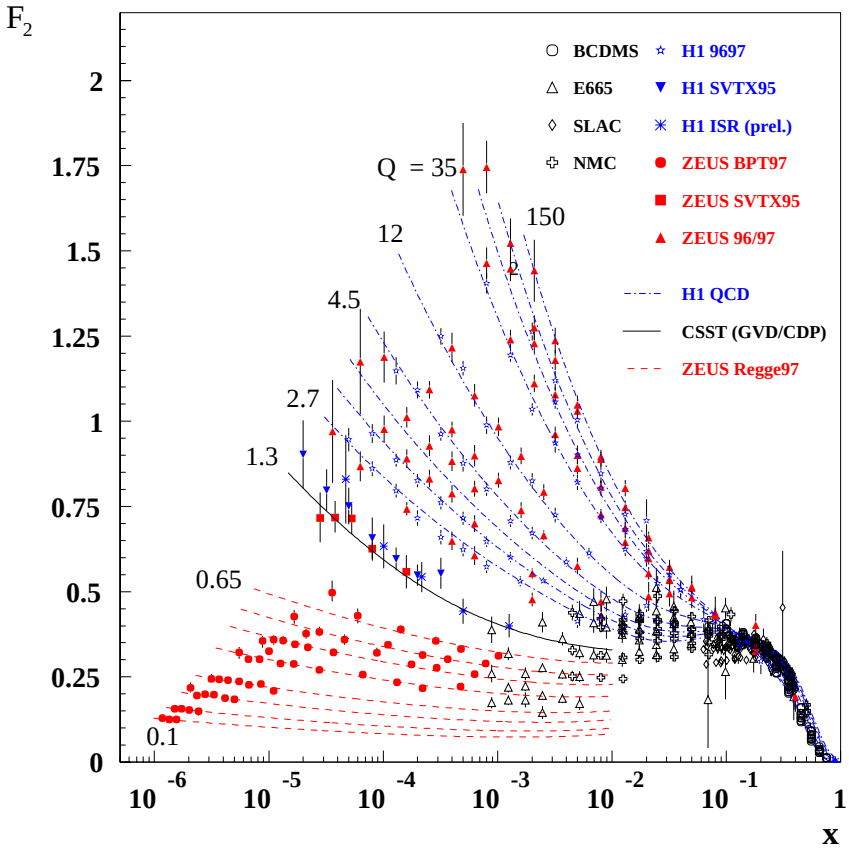


**Figure 19:** The structure function $\mathcal{F}_2$ as function of $x$ as measured by H1 and ZEUS and fixed target experiments for selected $Q^2$ between 0.1 and 150 GeV$^2$.

momentum densities - is observed: for fixed $Q^2$, $xg(x, Q^2)$ rises rapidly as $x \to 0$ and $\mathcal{F}_2$ and $xg$ rise by about the same factor.

Deep inelastic scattering at very high $Q^2$ is shown in Fig. 20 (right) in terms of $d\sigma(ep)/dQ^2$ for neutral-current (NC: $J = \gamma, Z$) and charged-current exchange (CC: $J = W^{\pm}$) as measured in $e^-p$ and $e^+p$ interactions [62, 63]. The NC cross sections are steeply falling with $Q^2$ as a result of the dominance of $\gamma$-exchange. At $Q^2 > 5000$ GeV$^2$, the contribution from $Z$-exchange becomes substantial. As a result of $\gamma - Z$ interference, the cross section for $e^-p$ scattering is larger than that for $e^+p$. The curves show the SM predictions which have uncertainties of 4% at $Q^2 = 400$ GeV$^2$ and 10% at $Q^2 = 10000$ GeV$^2$. The SM predictions agree well with the data. The comparison of the data with the SM predictions allow placing a lower limit of $7.3 \cdot 10^{-17}$ cm on the radius of quarks [63].

For CC scattering, a substantial difference between the $e^-p$ and $e^+p$ cross sections is observed which is due to the fact that different quark flavours are contributing. For $Q^2 > m_W^2$, the CC cross section reaches the same magnitude as the NC cross section: a

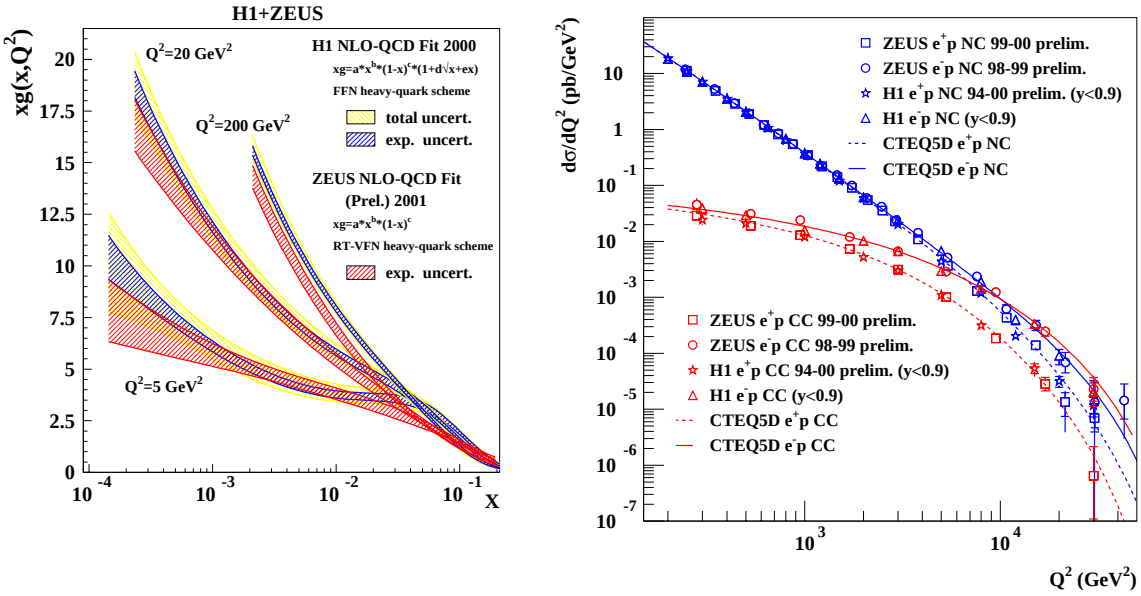


**Figure 20:** Left: The gluon momentum density of the proton as a function of $x$ as determined by H1 and ZEUS for $Q^2 = 5$, 20 and 200 GeV$^2$. Right:The neutral and charged current cross sections as measured in $e^-p$ and $e^+p$ scattering by H1 and ZEUS at high $Q^2$. The curves show the SM predictions.

striking example of electroweak unification! It is instructive to compare this result with typical electromagnetic and weak particle decays. There, the weak force is about ten orders of magnitude smaller than the electromagnetic one.

In Fig. 21 (left), the reduced CC cross section, $\tilde{\sigma}^{e^+p}_{CC} = \frac{2\pi x}{G_F^2}[\frac{m_W^2+Q^2}{m_W^2}]^2 \frac{d^2\sigma_{CC}}{dxdQ^2}$, is shown as a function of $x$ for different $Q^2$ intervals. The curves show that, at large $x > 0.1$, the contribution from $d$-quarks dominates. Given more luminosity, this offers the possibility of extracting the $d$-quark density directly from the data at high $Q^2$ where higher twist effects are negligible.

Diffraction represents a large fraction of hadronic interactions. Nevertheless, a rigorous description of diffraction within QCD is still missing. Diffraction in deep inelastic scattering seemed to be a remote subject at the beginning of HERA operation. Assuming (naively) the optical theorem to hold, the forward diffractive cross section for $\gamma^*p$ scattering can be deduced from the total $\gamma^*p$ cross section: $d\sigma_{diff}(t = 0)/dt \propto \sigma^2_{tot}$. For large c.m. energies $W \approx \sqrt{Q^2/x}$ is given by $\sigma_{tot} = \frac{4\pi^2\alpha}{Q^2}\mathcal{F}_2(x, Q^2)$. Since $\mathcal{F}_2$ is leading twist, the forward diffractive cross section is higher twist ($\propto 1/Q^4$) and was, therefore, expected to be negligible at large $Q^2$. The observation of DIS events with a large rapidity gap that represent a substantial fraction of the total cross section [64, 65] demonstrated that, on the contrary, inelastic diffraction plays an important role in DIS. In Fig. 21 (right), the ratio of the diffractive cross section for $\gamma^*p \to XN$ ($N$ = proton or low mass nucleon

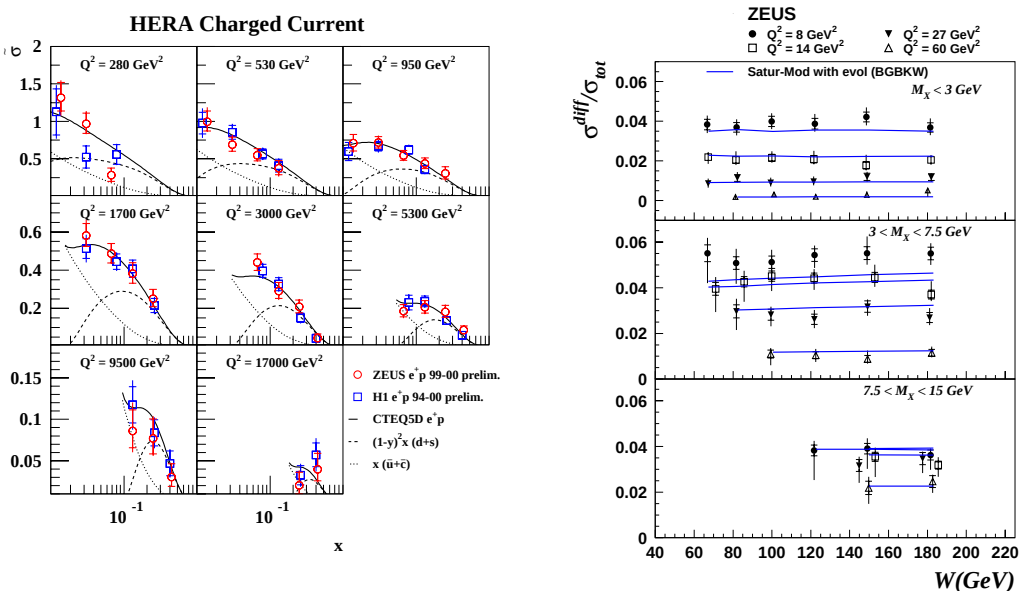


**Figure 21:** Left: The reduced cross section for $e^+p$ charged current scattering as measured by H1 and ZEUS. Right: The ratio of the diffractive cross section to the total cross section for different $m_X$ and $Q^2$ intervals as a function of $W$, as measured by ZEUS.

system) to the total $\gamma^* p$ cross section is shown as a function of $W$ for different $Q^2$ and $M_X$, the mass of $X$ [66]. The diffractive contribution is of the order of 10% or larger, viz. $\frac{\sigma_{diff}(M_X<15GeV)}{\sigma_{tot}} = 13.2 \pm 0.6\%, 9.4 \pm 0.6\%, 7.5 \pm 0.5\%$ at $Q^2 = 8$, 14, 27 GeV$^2$, respectively.

At HERA, diffraction can be studied in a systematic manner as a function of the resolution ($Q^2$), energy ($W$) and excitation ($M_X$). In modern language, HERA enables the determination of the diffractive structure function $F_2^{D(4)}(\beta, Q^2, x_{I\!P}, t)$ [67, 68] which is as fundamental a quantity as the inclusive structure function $F_2$. Here $\beta = Q^2/(Q^2 + M_X^2)$ is the diffractive analogue of the Bjorken scaling variable $x$, $x_{I\!P} = x/\beta$ and $t$ is the four momentum transfer squared to the proton. $Q^2$ and $\beta$ govern the QCD-evolution of $F_2^D$.

The authors of Ref. [69] have presented an interesting model for the description of diffraction in DIS. It considers diagrams of the type depicted in Fig. 17 (right) where the virtual photon turns into a $q\bar{q}$ or $q\bar{q}g$ state which then scatters on the proton. Fixing the free parameters from a comparison with the measured $\mathcal{F}_2$ data, this so-called Saturation Model makes absolute predictions for the diffractive cross section as a function of $Q^2, W$ and $M_X$. A recent calculation, which includes DGLAP evolution [70], gives a good account of the data, see the curves in Fig. 21 (right).

The process where diffraction might be studied at $Q^2 > 0$ in its most pure form is quasielastic or deeply virtual compton scattering (DVCS), $\gamma^* p \to \gamma p$. It promises also access to the skewed parton distributions. DVCS is a particularly difficult diffractive process to measure, firstly because its rate is small, and secondly because of the presence of a large background from the Bethe-Heitler process, $ep \to e\gamma p$. Figure 22 shows the first results

from H1 and ZEUS [71, 72] for the DVCS cross section as a function of $Q^2$ and $W$. The theoretical predictions [73, 74] (see curves) are in agreement with the measurements.

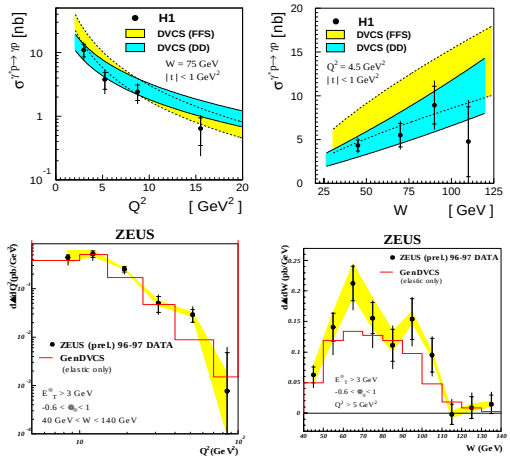


**Figure 22:** The cross section for deep inelastic virtual-photon compton scattering as a function of $Q^2$ and $W$, as measured by H1 and ZEUS.

The spin structure of the nucleon is investigated by HERMES which studies collisions of the polarized electron beam from HERA with a jet of polarized nuclei [77]. By comparing different hadronic final states, e.g. inclusive production of $\pi^+$ and $\pi^-$, information on the contribution to the nucleon spin from different quark flavours can be obtained. Figure 23 (left) shows the helicity asymmetry:

$$A_1^h = \frac{\sum_q e_q^2 \Delta q(x,Q^2) D_q^h(z)}{\sum_q e_q^2 q(x,Q^2) D_q^h(z)} \tag{10.2}$$

for the reaction $ed \to eh^{\pm}X$ as a function of $x$, summing over *all* hadron final states, and for those final states with a detected $h^+$ ($h^-$). The observed asymmetry is contributed almost solely by $h^+$ final states. From these data one concludes that the contributions to the nucleon spin: $\Delta u + \Delta\overline{u}$ is large and positive, $\Delta d + \Delta\overline{d}$ is small and negative, and the quark sea contribution is small, see Fig. 23 (right).

Sensitivity to the transverse polarization of quarks in the nucleon has been found in the study of single-spin asymmetries [75]. Figure 24 shows the analyzing power $A_{UL}^{sin\phi}$ as determined in an experiment where unpolarized positrons were scattered off longitudinally polarized protons and final state pions were detected as a function of the azimuthal angle $\phi$ around the direction of the virtual photon. The variable $z = E_\pi/\nu$ measures the fractional energy of the pion relative to that of the virtual photon. For $\pi^+, \pi^0$ the asymmetry $A^{sin\phi}$ is positive and growing with $z$ while for $\pi^-$ the asymmetry is small. This suggests that the single-spin asymmetries are associated with the valence quark distributions of the nucleon.

HERA II: During the past months HERA has been upgraded to increase the luminosity for the collider experiments by a factor of 3 - 5 to an instantaneous luminosity of $(5-7)\cdot 10^{31}$ cm$^{-2}$s$^{-1}$ by focussing the beams more strongly. Over the period 2002 -

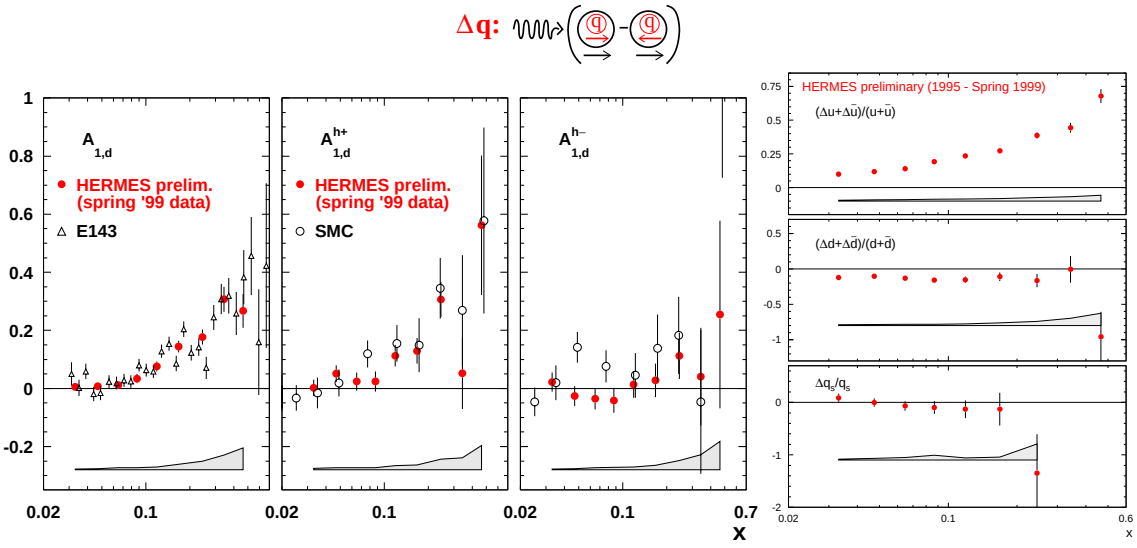


**Figure 23:** Left: The helicity asymmetry measured in $ed \to eh^{\pm}X$ reactions for all final states, for final states with an $h^+$ and for those with an $h^-$. Data from HERMES, E143 and SMC. Right: The relative contribution to the proton spin from different quark flavours as inferred from the analysis of the hadronic final state.

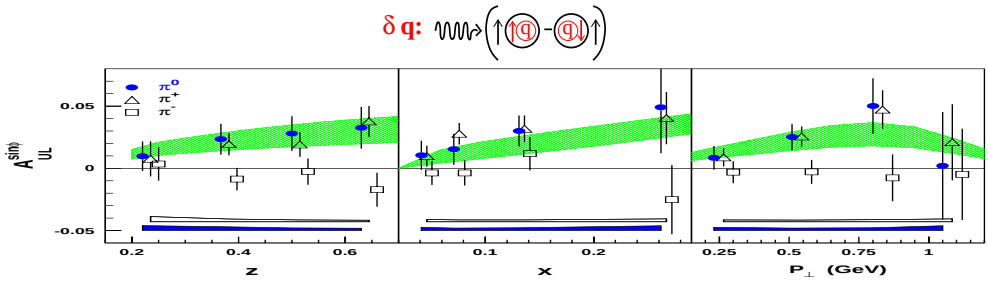


**Figure 24:** The transversity structure function as measured by HERMES.

2006, an integrated luminosity of 1 fb$^{-1}$ is expected per experiment. Spin rotators have been added for H1 and ZEUS so that interactions with left- and right-handed $e^-$ and $e^+$ can be studied separately. At the same time, H1 and ZEUS have improved (added) microvertexing to increase vastly the efficiencies for $c$ and $b$ quark tagging.

The physics aims [78] include precision measurements of the proton structure functions $F_2, F_L, xF_3, F_2^c, F_2^b$ for $Q^2 = 10 - 40000$ GeV$^2$; testing for quark substructure down to a few $10^{-17}$ cm; search with CC interactions for deviations from the SM down to $\Delta M_W = 60$ MeV; search for high mass $W$'s and $Z$'s up to 600 - 800 GeV; search for flavour changing neutral currents, e.g., $u \to c, t$. Furthermore, electron (positron) beams with definite helicity open the exciting possibility to measure the cross sections for $e_R^- p \to \nu X$ and $e_L^+ p \to \overline{\nu} X$ which are zero in the SM. Nonzero values would be a clear sign for new physics.

## 11. Heavy ion collisions at RHIC

The Relativistic Heavy Ion Collider RHIC at BNL gives access to new frontiers in the study of hadronic matter. RHIC extends the c.m. energy reach by an order of magnitude above that of the CERN-SPS. At sufficiently high energy densities Lattice QCD predicts a phase transition from hadronic matter to deconfined quarks and gluons. Whether the transition to the quark-gluon plasma takes place depends on the conditions of the matter created at the early stage of the collision. For instance, the ratio of baryon/antibaryon production at central rapidities is an important indicator for such a phase transition. For a pure quark/gluon plasma this ratio should be unity, or, in other words, the net baryon number should be zero.

RHIC has had a splendid start, providing Au-Au collisions at two-nucleon c.m. energies of $\sqrt{s_{NN}} = 130$ GeV with a luminosity of $2 \cdot 10^{25}$ cm$^{-2}$s$^{-1}$ which is 10% of the design luminosity. Data on particle production for central rapidities ($\eta \approx 0$) have been reported by the multi-purpose detectors PHENIX and STAR for integrated luminosities of several $\mu$b$^{-1}$[79].

The ratio of antiproton to proton production in the central region shows a dramatic increase from $N\overline{p}/Np = 0.00025$ at AGS ($\sqrt{s_{NN}} = 5$ GeV) and $\approx 0.07$ at SPS ($\sqrt{s_{NN}} = 17$ GeV) to RHIC where STAR has measured $N\overline{p}/Np \approx 0.6$ [80]. Figure 25 compares the $p_T$ spectra for $\pi^-$ and $\overline{p}$ as measured by PHENIX in the central region. For $p_T \approx 2.1$ GeV, an equal number of antiprotons and $\pi^-$ are produced!

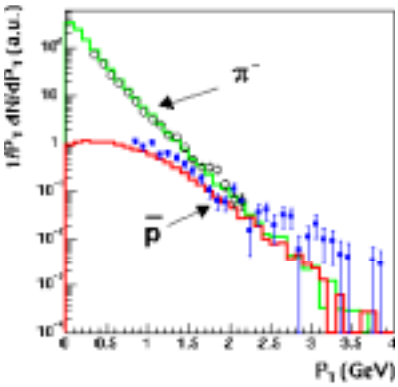


**Figure 25:** Comparison of $\overline{p}$ and $\pi^-$ yields in the central region as measured by PHENIX.

In Fig. 26 (left) the ratio of $h^-$ production in Au-Au collisions to $p\overline{p}$ collisions is compared at the same c.m. energy, $\sqrt{s_{NN}}$. For $p_T > 2$ GeV, one observes for Au-Au collisions the production of $h^-$ to be more and more suppressed relative to binary (= NN) collisions. The additonal energy density seen at RHIC is due mainly to an increase in particle production rather than to an increase of the transverse energy of the particles [81].

The azimuthal anisotropy of the transverse momentum distributions for noncentral collisions should be sensitive to the early evolution of the system. A measure for such an anisotropy is the second Fourier coefficient $v_2$, also called the elliptic flow. The measurement of $v_2$ versus $p_t$ from STAR, Fig. 26 (right), shows an almost linear rise up to $p_t = 1.5$

GeV, consistent with a hydrodynamic picture which predicts complete local thermalization. For $p_t > 2$ GeV saturation is observed which might signal the onset of hard processes in dense matter [82].

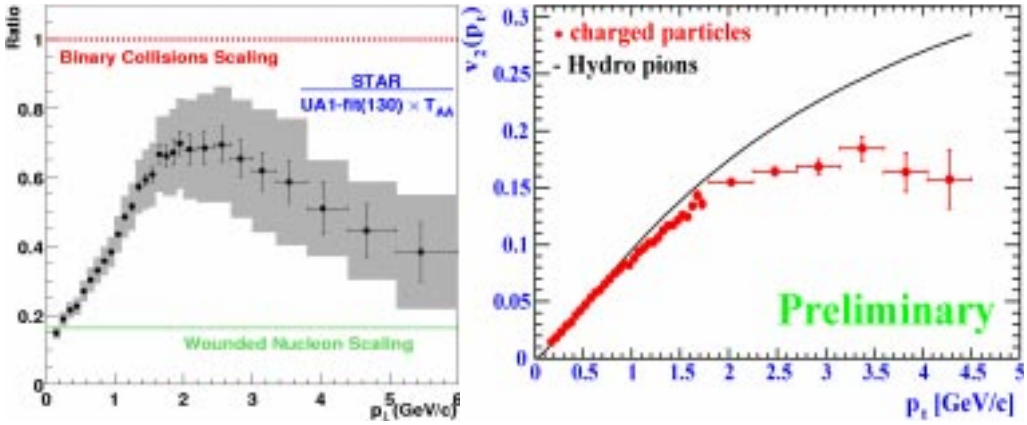


**Figure 26:** Left: The ratio of the particle yield measured by STAR (Au Au collisions) and UA1 ($\overline{p}p$ collisions) for central particle production. Right: The elliptic flow $v_2(t)$ versus $p_t$ for charged particles. From STAR.

## 12. Search for new physics at the TEVATRON

The new precision measurements of $M_W$ by CDF and D0 were perfomed by studying the $W \to e\nu, \mu\nu$ decay modes, as detailed in Fig. 27 (left). The $Z \to e^+e^-, \mu^+\mu^-$ decays combined with the known mass of the $Z$ provided a valuable means of calibration. The average value is $M_W = 80.0454 \pm 0.060$ GeV. The width of the $W$ was determined by D0 from the tail of the $W$ mass distribution, see Fig. 27 (right), resulting in

$$\Gamma_W = 2.231^{+0.145}_{-0.138}(stat) \pm 0.092(sys); \text{GeV}. \tag{12.1}$$

The SM prediction of $\Gamma_W^{SM} = 2.0937 \pm 0.0025$ GeV agrees with the measurement to within 1 s.d.

CDF searched for $\tilde{t}$ decaying via $\tilde{t} \to \tau b$ by $R_p$ parity violation. Figure 28 shows the distribution of the number of charged particles for the candidate events. Most events are accounted for by background from known $\tau\tau X$ final states. A lower limit of $M_{\tilde{t}} = 119$ GeV is obtained.

A heavy $W$ with standard decay into $e\nu$ should show up in the transverse mass $M_T$ of the system $(e\nu)$. The distribution of $M_T$ from the data is compared in Fig. 28 with the expected distributions for background contributions: no signal is observed. A similar analysis for the $\mu\nu$ system also led to a negative result. The combined $e\nu$ and $\mu\nu$ data yielded a lower limit of $M_{W'} < 786$ GeV.

Running has just started after the upgrade to TEVATRONII. The beam energy has been increased by 10% to 1 TeV. By storing more bunches the luminosity is expected to

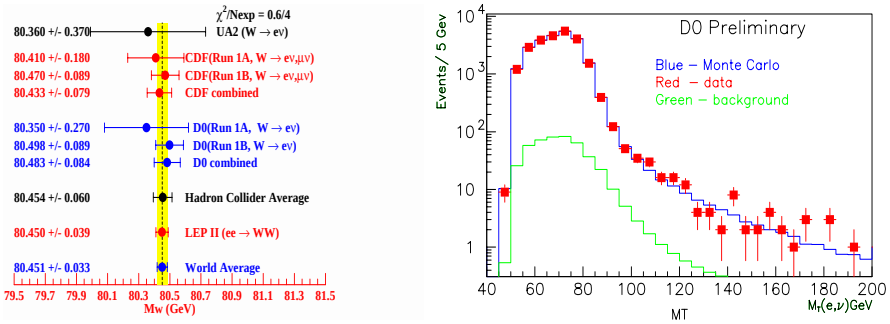


**Figure 27:** Left: Summary of $M_W$ values; Right: Spectrum of the transverse mass $M_T(e\nu)$ as measured by D0.

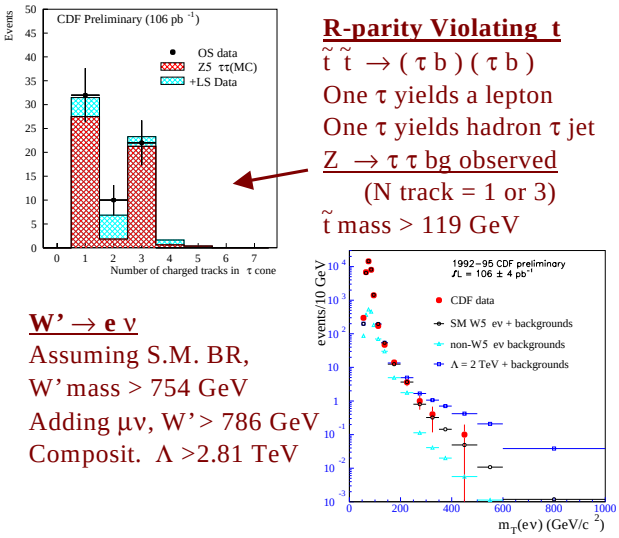


**Figure 28:** Search for $R_p$ -violating $t$ and for a heavy $W'$ performed by CDF.

increase by an order of magnitude to $10^{32}$ cm$^{-2}s^{-1}$. For the period 2002 - 7 the aim is to collect a total of 15 fb$^{-1}$ per experiment which is about a factor of 100 more than obtained in Run I.

What are the chances for CDF and D0 to see the Higgs? Figure 29 shows the sensitivity to the Higgs as a function of its mass. Run IIa should allow CDF and D0 to exclude masses up to 120 GeV at 3 s.d. or lead to a tantalizing bump. With the data expected from Run IIa+b the Higgs can be established with 3 (5) s.d., provided $M_H < 135$ GeV or $150 < M_H < 175$ GeV.

## 13. LHC

The LHC will open the door to physics at the multi-TeV scale. A few examples will illustrate its reach [83].

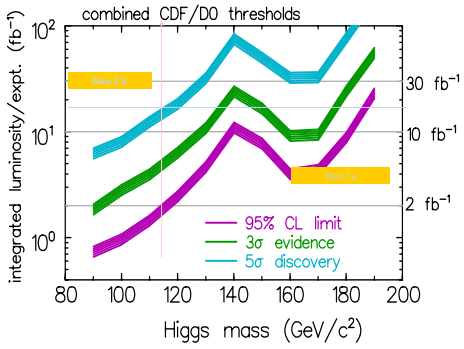


**Figure 29:** Sensitivity to the Higgs of CDF and D0 at TEVATRONII.

The Higgs can be detected over the full mass range starting from the lower limit of 114 GeV established by LEP up to the point where its width becomes of the order of its mass ($M_H \approx 1.3$ TeV ). Experimentally, the region of masses below 140 GeV is the most challenging one. Here detection via the $b\bar{b}$ and $\gamma\gamma$ decay channels is the most promising avenue. With 10 fb$^{-1}$ (corresponding to about one year running at $10^{33}$cm$^{-2}$s$^{-1}$) there is sufficient efficiency to discover the Higgs with 5 s.d. for masses between 114 GeV and 130 GeV, see Fig. 30 (left). At higher masses $WW^*(W)$ and $ZZ^*(Z)$ become the preferred decay channels, see Fig. 30 (right). In case there is no SM Higgs, its nonexistence can be established at the 95% level with data from less than a year's running.

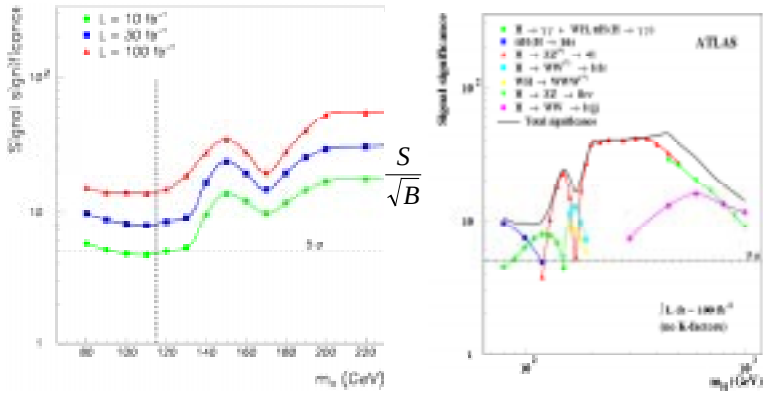


**Figure 30:** Discovery potential for the Higgs at the LHC. Shown is the significance of the signal in terms of the ratio $N_{Signal}/\sqrt{N_{background}}$ as a function of the Higgs mass.

The parameter space accessible in the search for SUSY particles is illustrated in Fig. 31 in terms of the parameters $m_{1/2}$ and $m_0$ for $\tan\beta = 10$. With data from a month of running squarks and gluinos can be discovered if their masses are below 1 TeV. The ultimate reach will be 2.5 - 3 TeV.

If extra dimensions do play a role, processes of the type $q+g \to q+G$, $G =$ graviton, are expected which produce events with jet + large missing tranverse energy. With 100 fb$^{-1}$ (corresponding to 1 year of running at $10^{34}$ cm$^{-2}$s$^{-1}$) sensitivity for extra dimensions up to

4 TeV can be reached. The production of a Graviton, e.g. in the process $gg \to G \to e^+e^-$, would be detected with a small background and its spin two could be established readily from its decay angular distribution (Fig. 31).

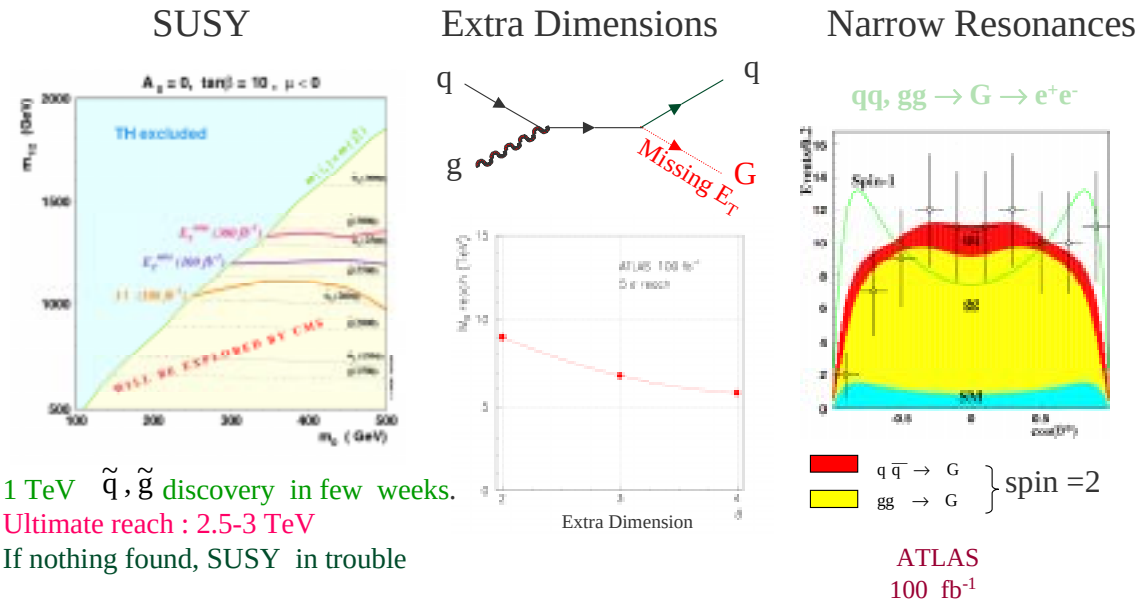


**Figure 31:** Discovery potential for new physics beyond the SM at the LHC.

## 14. TESLA

The tandem TEVATRON - LEP/SLC has amply demonstrated the power of a set up where a large hadron collider and an $e^+e^-$ collider are running concurrently and with comparable luminosity for elementary processes such as $q\overline{q}$ and $e^+e^-$ scattering at high energies. With the LHC under construction, it is essential to build also an $e^+e^-$ collider with 0.5 - 1 TeV c.m. energy for exploiting the new energy regime [84]. Given the high energy and the budgetary constraints, circular $e^+e^-$ machines are excluded because of their excessive beam radiation losses. The SLC at SLAC has demonstrated the technical feasibility of an $e^+e^-$ linear collider. Three linear collider projects for the 0.5 - 1 TeV regime have been studied over the past 10 - 15 years: NLC (SLAC) and JLC (KEK) - both with normal conducting cavities - and TESLA (DESY) with superconducting cavities. A concept suitable to enter the multi-TeV regime is under study at CERN (CLIC) with normal conducting cavities. At present the normal conducting cavity projects are faced with a technical problem at high accelerating gradients envisaged for the high end of the energy reach. The TESLA collaboration has demonstrated the feasibility of a superconducting solution and has prepared a technical design report for a machine with 500 - 800 GeV [85], which has been submitted to the German Government for evaluation.

The layout of TESLA is shown in Fig. 32. Two linacs with a total length of 33 km are pointed at each other. Two interaction points are foreseen. The expected luminosity of

$(3-6)\cdot 10^{34}\mathrm{cm}^{-2}\mathrm{s}^{-1}$ leads to about 300-500 $\mathrm{fb}^{-1}$/year. The energy reach is determined by the maximum accelerator gradient provided by the cavities. For operation at 500 (800) GeV a gradient of 23 (35) MV/m is required. By close collaboration with industry, industrially produced cavities (see Fig. 33) by now reach more than 25 GeV/m. With electropolishing, gradients in excess of 40 MV/m have recently been achieved for single cell cavities. A possible site for TESLA is shown in Fig. 33: the collider starts from the DESY premises towards the North. A test accelerator with the TESLA layout has been built at DESY by the TESLA collaboration and has now been operated for more than 9000 h. With this facility, the technical feasibility of the TESLA design has been established. The TESLA project includes an X-ray free electron laser for use in other scientific studies. X-ray free electron lasing in the 100 nm wave length regime has recently been demonstrated for the first time for these wave lengths [86, 87] and saturation (at a gain of $10^7$) has been reached for Self Amplified Stimulated Emission (SASE).

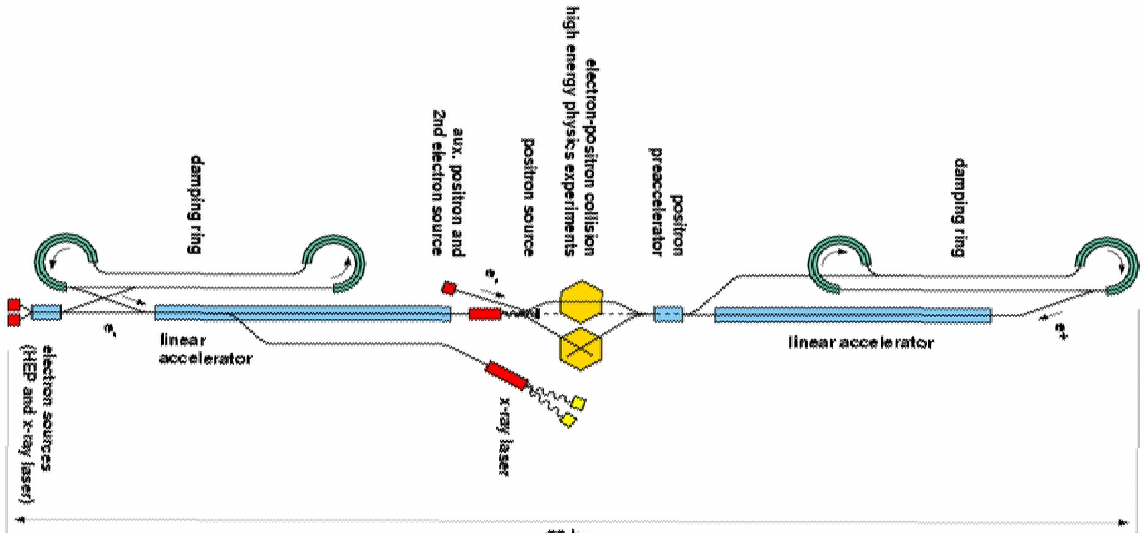


**Figure 32:** Layout of the TESLA collider.

A few examples may suffice to illustrate the physics reach of TESLA. The Higgs can be studied in a model independent way via associated production, $e^+e^- \to H^0 Z_{->\mu^+\mu^-}$, and can be directly detected – without further selection cuts – as a peak in the recoil spectrum of the $\mu^+\mu^-$ system sitting on top of a modest background (Fig. 34 (left)) [88]. At a c.m. energy of $\sqrt{s} = 350$ GeV and with 500 $\mathrm{fb}^{-1}$, 80000 Higgs are produced for $m_H = 120$ GeV. By requiring $Z$ to decay into $\mu^+\mu^-$, 4000 events are retained. The Higgs mass can be determined with a precision of 40 -100 MeV for $m_H \leq 180$ GeV. The Higgs decay modes and electroweak symmetry breaking effects can be studied in detail. The branching ratios can be measured with high precision as indicated by the size of the error bars in Fig. 34 (right). The measurement of the Higgs couplings to $t\bar{t}$ and $W\overline{W}$ will provide a precise test of an SM versus MSSM Higgs. This is illustrated in Fig. 35 (left).

In case there is no elementary Higgs, new physics must appear at the latest at a

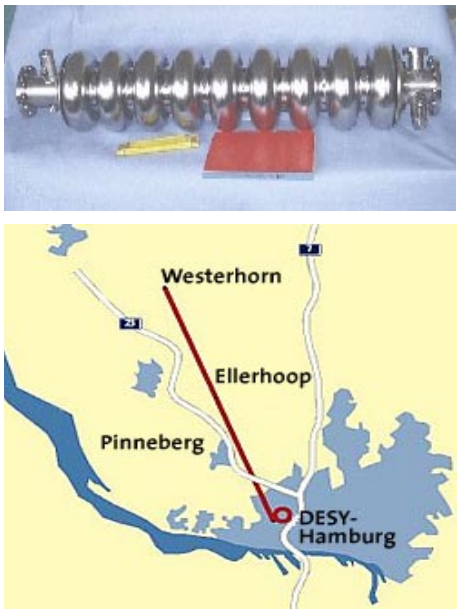


**Figure 33:** Possible site for TESLA (bottom) and a superconducting cavity of TESLA (top).

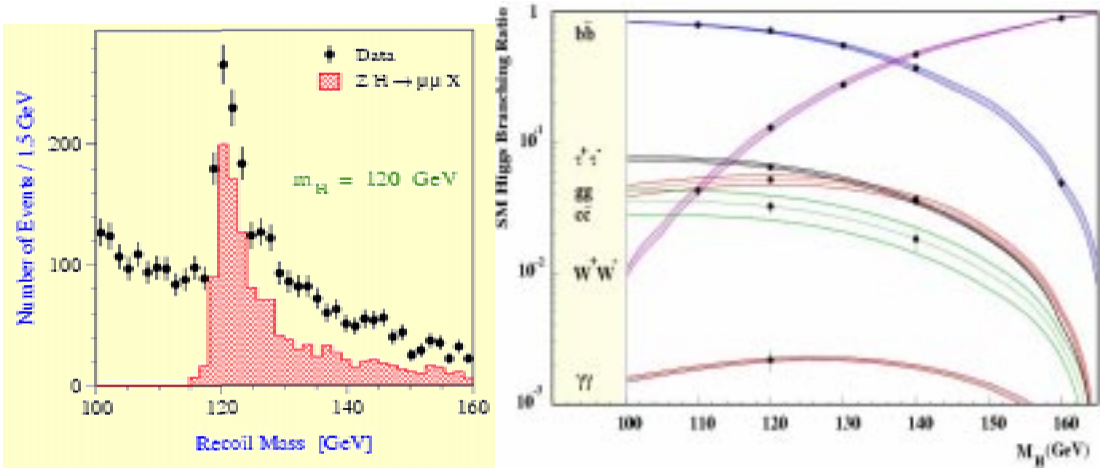


**Figure 34:** Left: Signal for the Higgs as measured by the mass of the system recoiling from the $\mu^+\mu^-$ pair in the reaction $e^+e^- \to H^0 Z_{->\mu^+\mu^-}$. Right: Expected Higgs branching ratios as a function of $m_H$; the expected experimental accuracy is indicated by the size of the error bars.

mass scale of about 1.2 TeV in order to unitarize $W_L W_L$ scattering [89]. Whatever this mechanism might be, TESLA will be sensitive to such a contribution, e.g., a strongly interacting vector state, up to a mass scale of 3-5 TeV [90].

As an example for manifestations of SUSY, Fig. 35 (right) shows the lepton energy spectrum arising from pair production of smuons, $e_R^- + e_L^+ \to \tilde{\mu}_R \tilde{\mu}_R$. The smuon mass can be reconstructed from the correlations between the two observed muons and from the endpoint of the $\mu$ energy spectrum [91]. Note that the lepton spectrum is almost

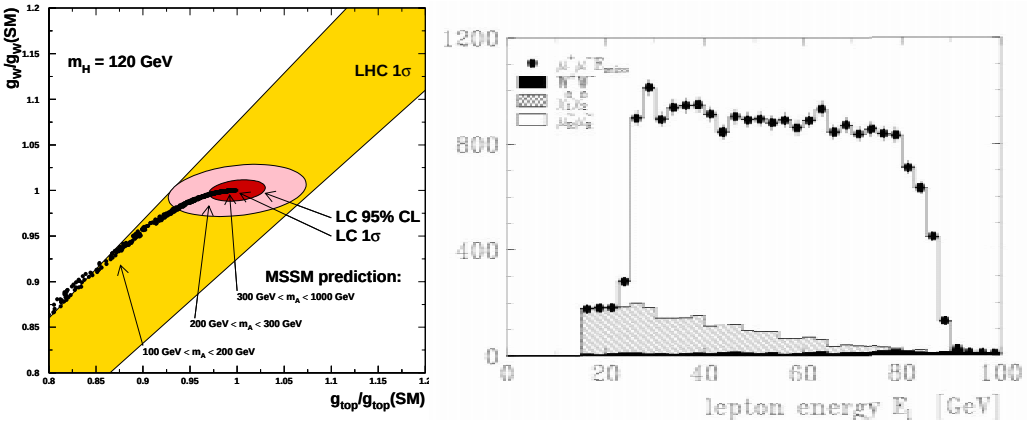


**Figure 35:** Left: Determination of the Higgs couplings $g_{ttH}$ and $g_{WWH}$ at TESLA compared to the SM and MSSM predictions for different values of the MSSM mass $M_A$. The broad error band shows the result expected from LHC. Right: Muon energy spectrum resulting from $e^-_R + e^+_L \to \tilde{\mu}_R\tilde{\mu}_R \to \mu^-\overline{\chi}^0_1\mu^+\overline{\chi}^0_1$ for $\sqrt{s} = 320$ GeV and 160 fb$^{-1}$.

background free. This is the message from many of such studies: in $e^+e^-$ collisions the background from SM processes is small.

The construction time for TESLA is estimated to be 8 years. If approved in 2003/4 operation could start in 2011/12. Approval of the project will need strong positive support by the HEP community worldwide [92] and will require that a substantial fraction of the components of the machine are provided by nonhost countries.

## 15. Summary of the summary

The high luminosity experiments BABAR and BELLE have opened a new window on the b-quark system and will revolutionize our knowledge of heavy quark systems. This conference has been presented with the discovery of CP violation in the $B$ system. The existence of direct CP violation in the $K$ system has been established. The results on solar neutrinos and the existing evidence from amospheric neutrinos have basically established that neutrinos do have a mass and do mix. When summed over all active neutrino flavours, the solar neutrino flux observed on earth agrees with the predicted flux. It is time to prepare for measuring the elements of the neutrino-CKM matrix which will require in the long run a neutrino factory. HERA is testing the space-like region at very large virtualities, while the low-x region has opened the door for the study of large parton densities and confinement in a novel way. Many more exciting results have been presented from dedicated machines, from large colliders, from nonaccelerator and from astrophysical experiments. Yet, the Standard Model again has defied all attemtps to look for physics beyond, with possibly one exception, the SM predictions for the $M_W$, $M_{top}$ mass relation. A reduction of the measurement errors for the $W$ and $t$ masses by a factor of two or more would increase the sensitivity for new physics greatly. We are all convinced that to look beyond requires higher

energies and are eagerly awaiting the turn-on of LHC and the approval and construction of an $e^+e^-$ collider in the 0.5 -1 TeV range.

## 16. Acknowledgements

We all have benefited at this conference tremendously from the hospitality, friendliness and dedication of our hosts and the wonderful atmosphere of Budapest. The technical support by Szabolcs Borsanyi (Budapest) was of great help for this talk. For providing information and figures I am indebted to H. Aihara, F. Bedeschi, T. Behnke, A. Blondel, R. Culbertson, W. deBoer, V.D. Elvira, M. Grünewald, P.M. Jacobs, E. Perez, R. McPherson, D. Plane, V.V. Derbo, Y. Suzuki, R. Tenchini, Y. Totsuka, N. Tuning, M. Vincter, J. Virdee, H. Wahl. Discussions with and advice from A. Ali, J. Bartels, W. Buchmüller, D. Cassel, D. Charlton, G. Chiarelli, L. Covi, K. Ganga, F. Jegerlehner, B. Klima, H. Kowalski, E. Lohrmann, K. Mönig, P. Schleper, S. Söldner-Rembold, J. Whitmore and P. Zerwas have been very helpful. Without the expert help from B. Löhr, S. Stonjek, B. Surrow and R. Wichmann the preparation of this talk would have been impossible.

## References

[1] BABAR Collaboration, B. Aubert et al., Phys. Rev. Lett. 87 (2001) 091801.

[2] BABAR Collaboration, Report presented by C. Touramanis at this conference.

[3] A. Ali and D. London, Eur. Phys. J. C18 (2001) 665, and private communication.

[4] E. Lunghi, Report presented at this Conference.

[5] Belle Collaboration, data provided by H. Aihara.

[6] Belle Collaboration, A. Abashian et al., Phys. Rev. Lett. 86 (2001) 2509 and S. Schrenk, Report presented at this conference.

[7] J.H. Christenson et al., Phys. Rev. Lett. 13 (1964) 138.

[8] KTeV Collaboration, Report presented at this conference.

[9] NA48 Collaboration, A. Lai et al., hep-ex/0110019, submitted to Eur. Phys. J.

[10] L. Wolfenstein, Phys. Rev. Lett. 13 (1964) 562.

[11] A. Buras, Lecture at KAON 2001, hep-ph0109197.

[12] M. Beneke, Report presented at this conference.

[13] SNO Collaboration, Q.R. Ahmad et al., Phys. Rev. 87 (2001) 07301, and A. McDonald, Report at this conference.

[14] Super-Kamiokande Collaboration, S. Fukuda et al., Phys. Rev. Lett. 86 (2001) 5651.

[15] C.E. Ortiz et al., Phys. Rev. Lett. 85 (2000) 2909.

[16] J.N. Bahcall, M.H. Pinsonneault and S. Basu, astro-ph/0010346 v2.

[17] J.N. Bahcall, Neutrino Astrophysics, 1989, Cambridge University Press.

[18] K. Nishikawa, Report presented at this conference.

[19] J. Wolf, Report presented at this conference.

[20] C. Weinheimer, Report presented at this conference.

[21] V.M. Lobashev et al., Proc. Int. Conf. Neutrino 2000, Sudbury, Canada.

[22] V. Aseev et al., "A next generation tritium beta decay experiment with sub-eV sensitivity for the electron neutrino mass", http://www.ik1.fzk.de/tritium.

[23] J. Bernabeu, Report presented at this conference.

[24] C. Gonzales-Garcia, Report presented at this conference.

[25] L. Wolfenstein, Phys. Rev. D17 (1978) 2369; S.P. Mikheyev and A. Y. Smirnov, Sov. J.Nucl. Phys. 42 (1985) 913.

[26] H. Fritzsch and Zhi-zhong Xing, contribution to this conference.

[27] Feasibility Study II of a muon based neutrino source, S. Ozaki et al., http://www.cap.bnl.gov/mumu/studyii/FS2-report.html

[28] A feasibility study of a neutrino factory in Japan, Y. Kuno et al., http://www-prism.kek.jp/nugactj/index.html

[29] Current Activities for a neutrino factory at CERN, R. Garoby, http://muonstoragerings.web.cern.ch/muonstoragerings/ Neutrino Factory: Beam and Experiments, A. Blondel et al., Nucl. Inst. Meth. Phys. Res., A451 (2000) 102.

[30] K. Ganga, Report presented at this Conference.

[31] L. Covi, Report presented at this conference.

[32] A recent formalism for analyzing the power spectrum can be found in S. Weinberg, astro-ph/0103281.

[33] R.A. Sunyaev and Y.B. Zeldovich, Astrophysics and Space Science, 7 (1970) 3.

[34] P.J.E. Peebles and J.T. Yu, Astrophys. Journal 162 (1970) 815.

[35] A.A. Penzias and R. Wilson, Astrophys. Journal 142 (1965) 419.

[36] G.F. Smoot et al, Astrophys. Journal 396 (1992) L1. C.L. Bennet et al.,Astrophys. Journal 464 (1996) 1.

[37] C.B. Netterfield et al., astro-ph/0104460 (2001).

[38] N.W. Halverson et al., astro-ph/0104489 (2001).

[39] A.T. Lee et al., astro-ph/0104459 (2001).

[40] X. Wang. M. Tegmark and M. Zaldarriaga, astro-ph/0105091 (2001).

[41] P. de Bernardis, http://oberon.roma1.infn.it/slides/ (2000).

[42] W. Venus, Report presented at this conference.

[43] D. Charlton, Report presented at this conference.

[44] ALEPH,DELPHI, L3 and OPAL Collaborations, The LEP working group for Higgs boson searches, CERN-EP/2001-055.

[45] A. Djouadi et al., Phys. Rev. D57 (1998)4179; S. Heinemeyer, W. Hollik and G. Weiglein, Eur. Phys. J. C9 (1999) 343.

[46] S. Heinemeyer and G. Weiglein, Proc. Int. Workshop on Linear Colliers, Fermilab, October 2000 and hep-ph/0012364.

[47] G. Altarelli et al., hep-ph/0106029 and JHEP 0106 (2001)018.

[48] P. Binetruy, Report presented at this conference.

[49] Muon g-2 Collaboration, H.N. Brown et al., Phys. Rev. Lett. 86 (2001) 2227.

[50] I. Logashenko, Report presented at this conference.

[51] A. Czarnecki and W.J. Marciano, hep-ph/0010194.

[52] M. Knecht et al., hep-ph/0111059.

[53] M. Knecht and A. Nyffeler, hep-ph/0111058.

[54] F. Jegerlehner, DESY 01-028 and hep-ph/0104304.

[55] F.J. Yndurain, Report presented at this conference.

[56] J.L. Feng and K.T. Matchev, Phys. Rev. Lett. 86 (2001) 3480; L.L. Everett et al., Phys. Rev. Lett. 86 (2001) 3484; E.A. Baltz and P. Gondolo, Phys. Rev. Lett. 86 (2001) 5004.

[57] H1 Collaboration, C. Adloff et al., DESY 00-181(2000); R. Wallny, Report presented at this conference.

[58] ZEUS Collaboration, J. Breitweg et al., Phys. Lett. B487 (2000) 53; S. Chekanov et al., Eur. Phys. J. C21 (2001) 3; A. Cooper-Sarkar and B. Surrow, Reports presented at this conference.

[59] V.N. Gribov and L.N. Lipatov, Soc.J. Nucl. Phys. 15 (1972) 438; ibid. 675.
L.N. Lipatov, Sov. J. Nucl. Phys. 20 (1975) 95.
Yu.L.Dokshitzer, Sov. Phys. JETP 46 (1977) 641.
G. Altarelli and G. Parisi, Nucl. Phys. B126 (1977) 298.

[60] K. Prytz, Phys. Lett. B311 (1993) 286; ibid. B332 (1994) 393.

[61] ZEUS Collaboration, data presented at DIS2001, 9th Int. Workshop on Deep Inelastic Scattering, Bologna (2001).

[62] H1 Collaboration, DESY 00-187 and Eur. Phys. J., to be published; H1 Collaboration, paper 787 submitted to this conference.

[63] ZEUS Collaboration, paper 602 contributed to this conference.

[64] ZEUS Collaboration, M. Derrick et al., Phys. Lett. B315 (1993) 481.

[65] H1 Collaboration, T. Ahmed et al., Nucl. Phys. B429 (1994) 277.

[66] ZEUS Collaboration, J. Breitweg et al., Eur. Phys. J. C6 (1999) 43.

[67] G. Ingelman and P. Schlein, Phys. Lett. B152 (1985) 256.

[68] J.C. Collins, Phys. Rev. D57 (1998) 3051; Err. ibid. D61 (2000) 019902.

[69] K. Golec-Biernat and M. Wüsthoff, Phys. Rev. D59 (1999) 014017; Phys. Rev. D60 (1999) 114023.

[70] J. Bartels, K. Golec-Biernat and H. Kowalski: H. Kowalski, Report presented at this conference.

[71] H1 Collaboration, C. Adloff et al., DESY 01-093 and Phys. Lett. B, to be published.

[72] ZEUS Collaboration, report presented by P. Saull at this conference.

[73] L.L. Frankfurt, A. Freund and M. Strikman, Phys. Rev. D58 (1998) 114001 and erratum Phys. Rev. D59 (1999) 119901E.

[74] A. Donnachie and H.G. Dosch, Phys. Lett. B502 (2001) 74.

[75] HERMES Collaboration, A. Airapetian et al., Phys. Rev. Lett. 84 (2000) 4047; Phys. Rev. D64: 097101 (2001)

[76] J. Stewart, Report presented at this conference.

[77] HERMES Collaboration, preliminary data presented by E.C. Aschenauer.

[78] Future Physics at HERA, Proc. Workshop 1995/6, ed. G. Ingelman, A. DeRoeck and R. Klanner.

[79] P.M. Jacobs, Report presented at this conference.

[80] STAR Collaboration, C. Adler et al., nucl-ex/0104022.

[81] in Au-Au collision PHENIX Collaboration, K. Adcox et al., Phys. Rev. Lett. 87 (2001) 052301.

[82] STAR Collaboration, C. Adler et al., nucl-ex/0107003.

[83] F. Gianotti, Report presented at this conference.

[84] See ECFA resolution presented by L. Foa at this conference.

[85] TESLA Technical Design Report, DESY 2001-011, ECFA 2001-209, March 2001.

[86] J. Andruszkow et al., Phys. Rev. Lett. 85 (2000) 3825.

[87] S.V. Milton et al., Phys. Rev. Lett. 85 (2000) 988.

[88] TESLA Technical Design Report vol. III, p.14 ff.

[89] B.W. Lee, C. Quigg and H.B. Thacker, Phys. Rev. Lett. 38 (1977) 883, Phys. Rev. D16 (1977) 1519; T. Appelquist and M.S. Chanowitz, Phys. Rev. Lett. 59 (1987) 2403; M.C. Chanowitz, Ann. Rev. Nucl. Phys. 38 (19xx) 323.

[90] TESLA Technical Design Report vol. III, p.101 ff.

[91] TESLA Technical Design Report vol. III, p.57 ff.

[92] See statement by HEPAP Subpanel on Long Range Planning for U.S. High-Energy Physics, draft report 29 October 2001: http://doe-hep.hep.net/lrp_panel/index.html;
and ACFA statement: http://ccwww.kek.jp/acfa/document/2ndLC.html